nature communications

Article

https://doi.org/10.1038/s41467-025-59307-y

# DHODH modulates immune evasion of cancer cells via CDP-Choline dependent regulation of phospholipid metabolism and ferroptosis

Received: 29 February 2024

Accepted: 15 April 2025

Published online: 24 April 2025

Check for updates

Da Teng[1,2], Kenneth D. Swanson[2], Ruiheng Wang[1,2], Aojia Zhuang[1], Haofeng Wu[2], Zhixin Niu[3], Li Cai[4], Faith R. Avritt[5], Lei Gu[3], John M. Asara[6], Yaqing Zhang[7] & Bin Zheng[1,2]

The ability of cancer cells to evade immune destruction is governed by various intrinsic factors including their metabolic state. Here we demonstrate that inactivation of dihydroorotate dehydrogenase (DHODH), a pyrimidine synthesis enzyme, increases cancer cell sensitivity to T cell cytotoxicity through induction of ferroptosis. Lipidomic and metabolomic analyses reveal that DHODH inhibition reduces CDP-choline level and attenuates the synthesis of phosphatidylcholine (PC) via the CDP-choline-dependent Kennedy pathway. To compensate this loss, there is increased synthesis from phosphatidylethanolamine via the phospholipid methylation pathway resulting in increased generation of very long chain polyunsaturated fatty acid-containing PCs. Importantly, inactivation of *Dhodh* in cancer cells promotes the infiltration of interferon γ-secreting $CD8^+$ T cells and enhances the anti-tumor activity of PD-1 blockade in female mouse models. Our findings reveal the importance of DHODH in regulating immune evasion through a CDP-choline dependent mechanism and implicate DHODH as a promising target to improve the efficacy of cancer immunotherapies.

Evading immune destruction is a hallmark of cancer[1]. Anti-tumor immune surveillance represents one of the most significant selection pressures against tumor initiation and progression and is thus a potential vulnerability for exploitation in cancer prevention and treatment. Various oncogenes and tumor suppressors in cancer cells have been shown to influence the immune contexture of the tumor microenvironment and modulate the anti-tumor activity of cytotoxic cells[2]. Such tumor-intrinsic mechanisms that are required for immune evasion also play critical roles in determining the responses to various cancer therapies, including immune checkpoint blockade[3]. In addition to the well-established roles in controlling their growth and proliferation, metabolic alterations in cancer cells also influence the metabolic state of the tumor micro-environment and contribute to immune evasion[2]. However, the regulation of T cell cytotoxicity by metabolic processes in cancer cells is still understudied.

[1]Cedars-Sinai Cancer Institute, Department of Biomedical Sciences, Cedars-Sinai Medical Center, Los Angeles, USA. [2]Cutaneous Biology Research Center, Massachusetts General Hospital and Harvard Medical School, Charlestown, Massachusetts, USA. [3]Epigenetics Laboratory, Max Planck Institute for Heart and Lung Research, Bad Nauheim, Germany. [4]Department of Cancer Biology, University of Texas MD Anderson Cancer Center, Houston, TX, USA. [5]College of Literature, Science, and the Arts, University of Michigan, Ann Arbor, MI, USA. [6]Division of Signal Transduction, Beth Israel Deaconess Medical Center and Department of Medicine, Harvard Medical School, Boston, Massachusetts, USA. [7]Department of Surgery, University of Michigan, Ann Arbor, MI, USA. e-mail: bin.zheng@cshs.org

Dihydroorotate Dehydrogenase (DHODH) catalyzes the conversion of dihydroorotate to orotate, a rate-limiting step in the de novo pyrimidine nucleotide synthesis pathway. Pyrimidine synthesis provides precursors used in DNA and RNA that are critical for cell growth and proliferation. In addition, pyrimidines are used essential for protein and lipid glycosylation, glycogen synthesis, and phospholipid biosynthesis. DHODH is the only known enzyme in the pyrimidine synthesis pathway known to be localized to the mitochondria and is functionally linked to the mitochondrial complex III where it contributes to mitochondrial respiration-dependent cell growth by providing reduced CoQ10[4,5]. Various studies have shed light onto a critical role of DHODH in the initiation and progression of cancer[6–14]. DHODH was found to be important for the transcriptional elongation of genes that are critical for melanoma growth[6]. Inhibition of DHODH induces myeloid differentiation in acute myeloid leukemia models, representing a promising strategy for overcoming differentiation blockade[7]. In addition, DHODH was suggested to be a therapeutical target in PTEN-deficient cancer[8], triple-negative breast cancer[9], KRAS-driven cancer[10], glioblastoma stem cells[11], small cell lung cancer[12], MYC- amplified medulloblastoma[13] and IDH mutant glioma[14]. Despite promising activities of pharmacological inhibitors of DHODH (DHODHi) in various preclinical cancer models, the clinical prospect of DHODHi for cancer treatment is still unclear. A better understanding of the tumor-intrinsic role of DHODH in immune evasion and the effect of DHODHi on the tumor microenvironment will likely facilitate future clinical development of DHODHi for cancer treatment.

Here we report that CRISPR-mediated knockout (KO) of DHODH in mouse cancer cells inhibited the growth of tumors in immune competent mice, but not in immune-deficient NSG mice. Inhibition of DHODH in cancer cells or treatment with the DHODHi, brequinar (BRQ) increased their sensitivities to $CD8^+$ T cell mediated killing through induction of ferroptosis. Intriguingly, lipidomic and metabolomic analyses revealed that BRQ treatment reduces CDP-choline level and shifts the synthesis of PC from the CDP-choline dependent Kennedy pathway to the phosphatidylethanolamine (PE) methylation pathway that results in increased generation of very long chain polyunsaturated fatty acid-containing PCs. Supplementation of CDP-choline in cancer cells reversed this increase in longer chain polyunsaturated fatty acid-containing PC levels, upregulation of ferroptosis, and enhancement of $CD8^+$ T cell mediated killing induced by BRQ treatment. Importantly, inactivation of DHODH in cancer cells or BRQ treatment promoted the infiltration of IFNγ-secreting $CD8^+$ T cells and enhanced the anti-tumor activity of PD-1 blockade in syngeneic mouse tumor models. Moreover, spatial transcriptomic analysis suggests an inverse correlation of DHODH expression level and cytotoxic T cell infiltration in human cancer tissues. Our findings not only support that DHODH plays a critical role in regulating immune evasion, but also reveals a novel regulatory mechanism whereby alterations in CDP-Choline can effect ferroptosis.

## Results

### DHODH in cancer cells modulates their sensitivity to T cell cytotoxicity

To investigate the tumor-intrinsic role of DHODH in immune evasion, we generated CRISPR-Cas9-based *Dhodh* knockout (DHODH KO) in D4M mouse melanoma cells[15] and compared the growth of their allografted tumors in NOD *scid* gamma (NSG) immune-deficient to those in immune-competent syngeneic C57BL/6 WT mice. Strikingly, we found that knockout of DHODH strongly inhibited the growth of tumors in immune competent C57BL/6 mice, but not in immune-deficient NSG mice (Fig. 1A, B and Supplementary Fig. 1A, B). In DHODH KO tumors grown in C57BL/6 mice, we also observed higher levels of $CD8^+$ T cell infiltration and a higher percentage of $IFN\gamma^+$ $CD8^+$ T cells when compared to DHODH WT control tumors (Fig. 1C, D, Supplementary Figs. 1D and 8). We therefore examined the effects of the DHODH inhibitor, BRQ on allografted WT tumor growth in immune-competent mice implanted with syngeneic mouse cancer cells. After pilot studies, we chose a much lower dose of BRQ (5 mg/kg), as compared to 25-50 mg/kg in other recent mouse studies[7,12,16] to avoid the potential concern of toxicity that were observed from prior clinical development of this drug for cancer treatment[17,18]. As shown in Supplementary Fig. 1E, H and I, this lower dose retained significant anti-tumor growth effects of BRQ in D4M, YUMMER1.7, and MC38 models. Interestingly, like our results with DHODH KO tumors, we found that BRQ treatment significantly increased $CD8^+$ T cell infiltration in BRQ-treated tumors (Supplementary Fig. 1J, K). Moreover, similar to DHODH KO, BRQ treatment had much stronger anti-tumor effects in immune-competent wildtype C57BL/6 mice than in NSG mice (Supplementary Fig. 1E–G). These results strongly suggest that the stimulation of anti-tumor immunity is critical for the anti-tumor effects of DHODH inhibition.

Next, to further test the tumor-intrinsic role of DHODH in regulating tumor immune evasion, we examined the effects of DHODH inhibition in cancer cells on their susceptibility to $CD8^+$ T cell mediated tumor cell killing in vitro. MC38 mouse colon cancer cells expressing ovalbumin (OVA) were treated for 1 μM BRQ or DMSO vehicle control for 24 h before incubation with OT-1 transgenic $CD8^+$ T cells. The killing of cancer cells by T cells was monitored by flow cytometry and normalized to parallel treated cultures in the absence of T cells. As shown in Fig. 1E and Supplementary Fig. 1L, BRQ pre-treatment greatly enhanced the antigen-specific killing activity of $CD8^+$ T cells towards tumor cells. Knockout of *Dhodh* in MC38-OVA cells notably inhibited their tumor growth in immune-competent syngeneic C57BL/6 WT mice (Supplementary Fig. 1A, B, and 1M). Similar effects of BRQ were observed in D4M (Fig. 1F) and M14 human melanoma cells (Supplementary Fig. 1N) in non-antigen-specific killing assays. Supplementation of D4M, or MC38-OVA cells with uridine fully rescued the enhanced killing of cancer cells by $CD8^+$ T cells in the presence BRQ (Fig. 1G), suggesting the on-target effects of BRQ on inhibiting DHODH and subsequent suppression of pyrimidine synthesis was responsible for these results.

In addition to pharmacological inhibition of DHODH, we also carried out similar experiments in D4M and MC38-OVA cells with CRISPR-mediated DHODH ablation and observed similar effects on $CD8^+$ T cell mediated tumor cell killing (Fig. 1H). Moreover, we monitored the expression of various $CD8^+$ T cell activation markers by flow cytometry to examine alterations in their functional status following incubation with tumor cells pre-treated with BRQ or vehicle control. We found that pretreatment of tumor cells with BRQ led to higher levels of CD69, IFNγ, CD107a, and granzyme B expression in co-cultured $CD8^+$ T cells, consistent with higher levels of cytotoxicity (Fig. 1I–L). These results suggest that inhibition of DHODH in tumor cells increases their susceptibility to $CD8^+$ T cell-mediated cytotoxicity and led to higher levels of T cell activation.

### Ferroptosis is critical for DHODH inhibitor-induced enhanced sensitivity to $CD8^+$ T cell cytotoxicity

Inactivation of DHODH was recently demonstrated to induced ferroptosis, an iron-dependent cell death induced by excessive phospholipid peroxidation[19], through a mitochondrial CoQ10-dependent mechanisms in cancer cells[20]. Therefore, we investigated whether the possible involvement of ferroptosis in sensitizing them to $CD8^+$ T cell-mediated cytotoxicity by DHODH inhibition. We first confirmed that knockout of *Dhodh* or inhibition of DHODH by the small molecule inhibitors, BRQ, BAY2402234[21], PCT299[22], and ASLAN003[23], all increased levels of lipid peroxidation as measured by BODIPY C11 or 665/676 staining (Fig. 2A–C, Supplementary Figs. 1C, 2A, B and 9A, 9C). As expected, both DHODH KO and DHODH inhibition induced ferroptotic cell death, which was reversed by co-treatment with the ferroptosis inhibitor ferrostatin-1 (Fer-1) (Supplementary Figs. 2C, D and

https://doi.org/10.1038/s41467-025-59307-y

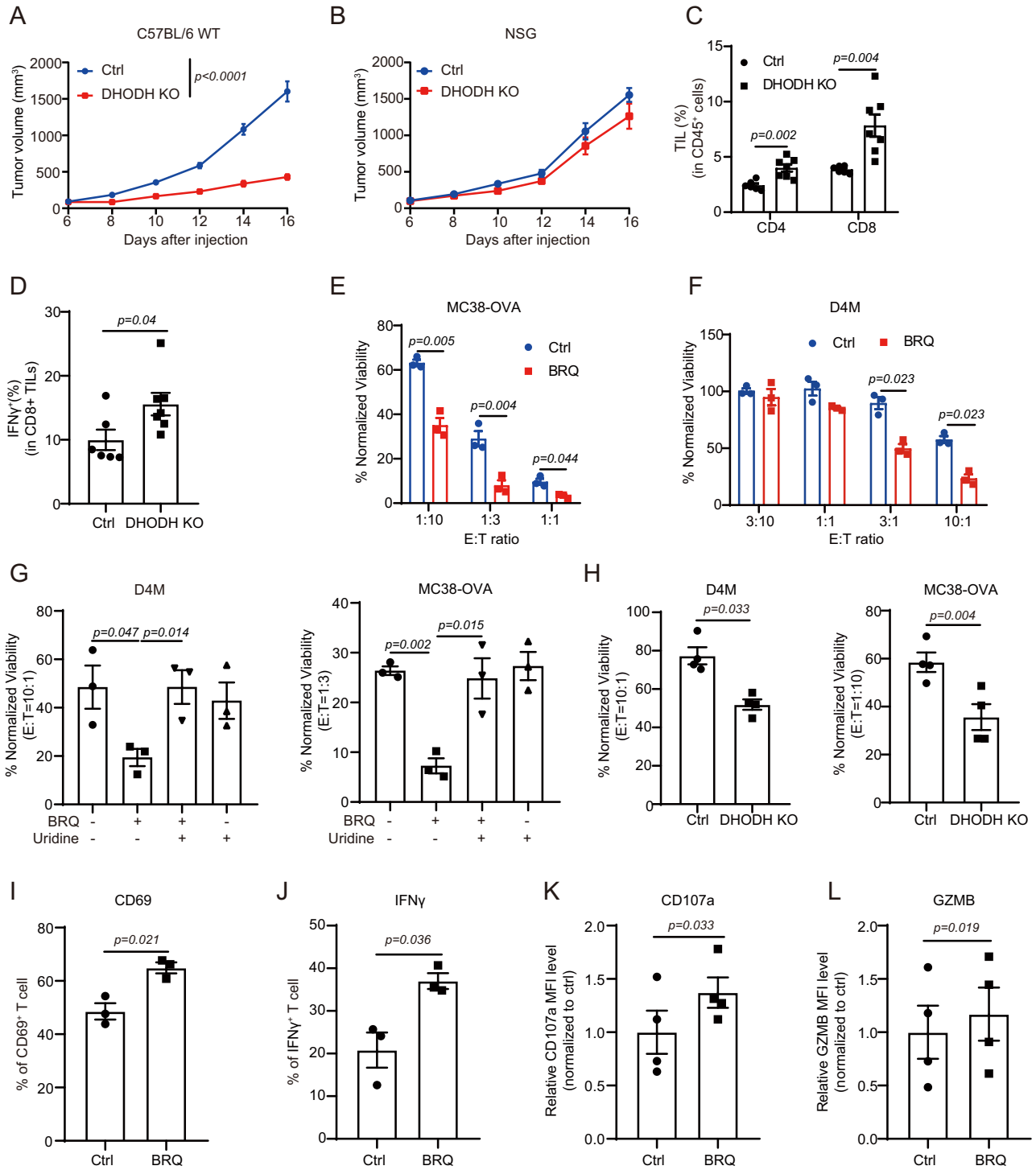


**Fig. 1 | DHODH in cancer cells modulates their sensitivity to T cell cytotoxicity.** **A**, **B** Measurements of flank tumors established using either control (Rosa26 gRNA) or DHODH KO D4M cells grown in either C57BL/6 mice (**A**, $n = 6$ mice for Ctrl group and $n = 7$ mice for DHODH KO group) or NSG mice (**B**, $n = 6$ mice for each group). **C** Analysis of tumor-infiltrating T cells revealed a significant increase in $CD4^+$ and $CD8^+$ T cells in the DHODH KO D4M tumors in C57BL/6 mice (Ctrl group, $n = 6$; DHODH KO group, $n = 7$). **D** $CD8^+$ T cells isolated from DHODH KO D4M tumors in C57BL/6 mice showed increased IFNγ expression (Ctrl group, $n = 6$; DHODH KO group, $n = 7$). **E**, **F** Pre-treatment of MC38-OVA (**E**) or D4M (**F**) cells with 1 μM BRQ for 24 h resulted in increased susceptibility to subsequent killing by activated OT−1 or WT $CD8^+$ T cells, respectively, at the indicated effector cell: target cell ratios (E:T). Data were normalized to parallel cultures treated without T cells ($n = 3$ biologically independent experiments). **G** Uridine supplementation rescues BRQ-induced susceptibility to $CD8^+$ T cell killing in D4M (left) and MC38-OVA (right) cells ($n = 3$ biologically independent experiments). **H** Knockout of DHODH in D4M (left) and MC38-OVA cells (right) also resulted in increased susceptibility to $CD8^+$ T cell cytotoxicity in vitro ($n = 4$ biologically independent experiments). **I**–**L** 1 μM BRQ resulted in higher levels of CD69 (**I**), IFNγ (**J**), CD107a (**K**) and GZMB (**L**) in murine $CD8^+$ T cells that were co-cultured with D4M cells pre-treated with compared to those co-cultured with DMSO treated D4M cells (**I** and **J**, $n = 3$; **K** and **L**, $n = 4$ biologically independent experiments). For panels **A**, **B**, the adjusted $p$ values were calculated using a two-sided Tukey's multiple comparisons test. For panels **C**, **D**, $p$ values were calculated by unpaired two-tailed Student's t-tests. For other panels, $p$ values were calculated by paired two-tailed Student's t-tests. Data are represented as mean ± SEM. Source data are provided as a Source Data file.

https://doi.org/10.1038/s41467-025-59307-y

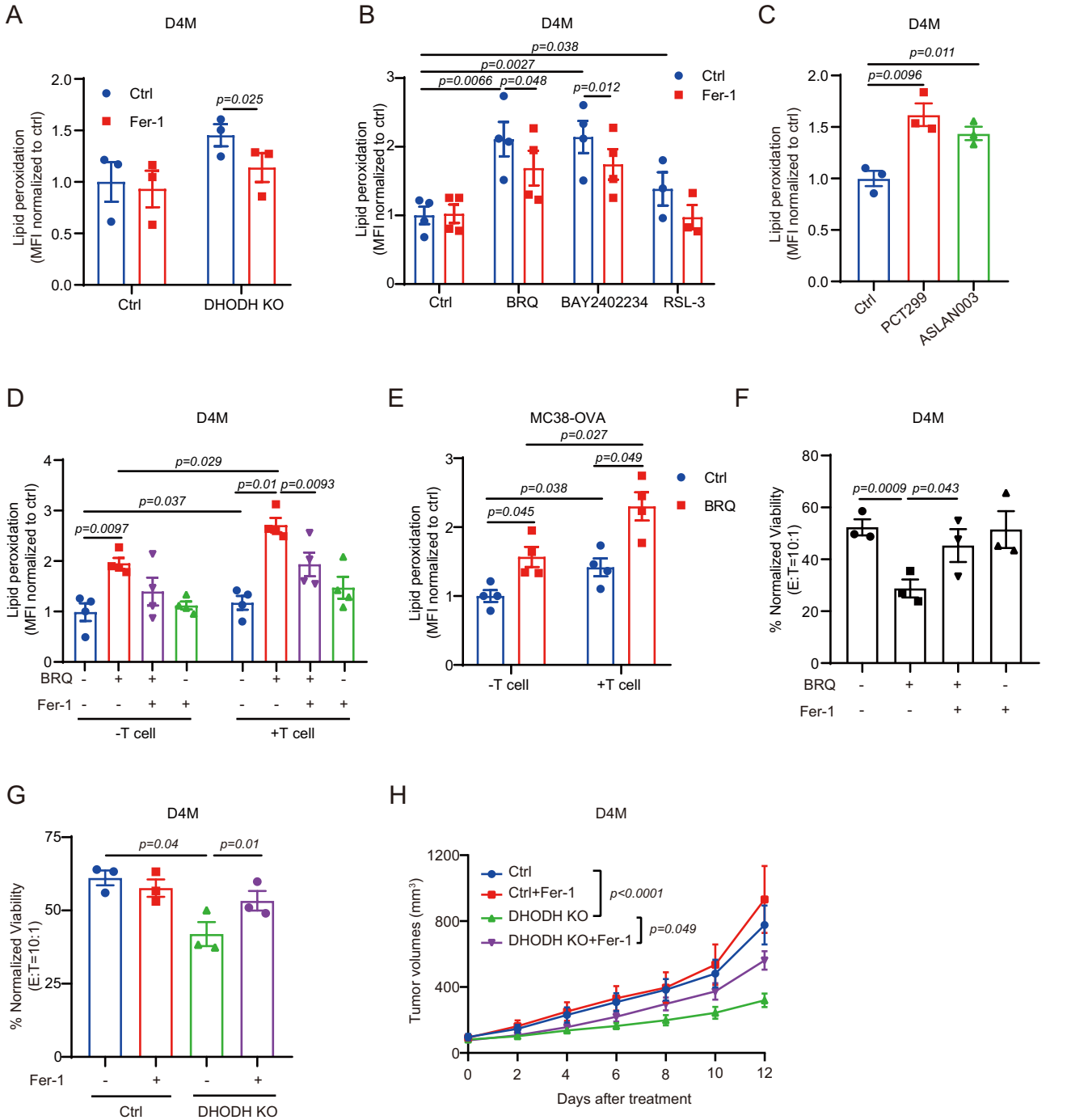


**Fig. 2 | Ferroptosis is critical for DHODH inhibitor-induced enhanced sensitivity of tumor cells to T cell cytotoxicity. A** Knockout of *Dhodh* in D4M cells results in increased lipid peroxidation that was reversible by Fer-1 co-treatment ($n = 3$ biologically independent experiments). **B** Treatment of D4M with 1 μM BRQ, 10 nM BAY2402234, or 1 μM RSL-3 for 24 h increased lipid peroxidation in a Fer-1 sensitive manner ($n = 4$ for ctrl, BRQ and BAY2402234 group; $n = 3$ for RSL-3 group, biologically independent experiments). **C** Treatment of D4M with 10 μM PCT299, or 1 μM ASLAN003 for 24 h increased lipid peroxidation ($n = 3$ biologically independent experiments). **D** Co-culture of CD8$^+$ T cell further increased lipid peroxidation in BRQ treated D4M cells in a Fer-1-sensitive manner ($n = 4$ biologically independent experiments). **E** Lipid peroxidation in BRQ-pre-treated MC38-OVA cells was also increased upon CD8$^+$ T cell co-culture. Cells were pre-treated DMSO, 1 μM BRQ, 20 μM Fer-1, or BRQ with Fer-1 for 24 h and then co-cultured with activated splenic CD8$^+$ T cells at indicated E:T ratio for 24 h followed by FACS measurement of lipid peroxidation of tumor cells using BIODPY C11 or 665/676 ($n = 4$ biologically independent experiments). Data for panels **D** and **E** were normalized to parallel DMSO-treated tumor cells cultures in the absence of T cells. **F** Effect of pre-treatment of D4M cells with DMSO, 1 μM BRQ, 20 μM Fer-1, or BRQ with Fer-1 for 24 h on CD8$^+$ T cell mediated cytotoxicity ($n = 3$ biologically independent experiments). **G** Fer-1 rescued the effect of *Dhodh* knockout on CD8$^+$ T cell mediated cytotoxicity ($n = 3$ biologically independent experiments). **H** Fer-1 promoted the growth of D4M DHODH KO tumors in C57BL/6 mice ($n = 7$ for each group). 5 mg/kg of Fer-1 or DMSO was administered intraperitoneally every second day to mice implanted with the indicated tumor cell lines. For panel **H**, the adjusted *p* values were calculated using a two-sided Tukey's multiple comparisons test. For other panels, *p* values were calculated by paired two-tailed Student's t-tests. Data are represented as mean ± SEM. Source data are provided as a Source Data file.

9B, 9D). Next, we measured lipid peroxidation of tumor cells in the presence or absence of $CD8^+$ T cells. Consistent with previous findings[24], exposure of D4M or MC38-OVA tumor cells to activated $CD8^+$ T cell alone led to increases of lipid peroxidation levels, which was further increased by pretreatment of tumor cells with BRQ in the presence of $CD8^+$ T cells (Fig. 2D, E and Supplementary Fig. 2E). As expected, these increases in lipid peroxidation levels were sensitive to Fer-1 (Fig. 2D). Importantly, treatment of tumor cells with Fer-1 significantly reversed the increased sensitivity to $CD8^+$ T cell-mediated killing in both BRQ treated and DHODH KO cells (Fig. 2F, G and Supplementary Fig. 2F, G). Moreover, Fer-1 treatment also significantly reversed the effects of DHODH KO on D4M tumor growth in mice (Fig. 2H). Together, these results support that DHODH inhibition-induced ferroptosis sensitized these cells to $CD8^+$ T cell cytotoxicity.

### DHODH inhibitor treatment altered phosphatidylcholine metabolism and reduced CDP-choline levels

We next carried out lipidomic profiling analysis to investigate the mechanisms underlying the effects of DHODH inhibition that drives lipid peroxidation. D4M melanoma cells were treated with 1 μM BRQ for 24 h followed by lipid extraction using methyl tert-butyl ether and mass spectroscopy analysis. We did not observe significant impact of BRQ on the relative distribution of the major classes of phospholipid (Fig. 3A). The total levels of PC and phosphatidylethanolamine (PE), two of the most abundant cellular phospholipids did not change markedly upon BRQ treatment (Fig. 3B). Since fatty acid chain elongation is known to regulate ferroptosis[19,25], we analyzed the effects of BRQ on fatty acid chain length in PC and PE. We found that BRQ treatment led to a significant increase in the levels of PC with very long chain fatty acid (VLCFA, carbon > 21), and a decrease in those with long chain fatty acid (LCFA, carbon between 13 and 21) (Fig. 3C and Supplementary Fig. 3A). Interestingly, this change in the ratio of VLCFA to LCFA upon BRQ treatment occurred only in PC, but not PE (Fig. 3D, E and Supplementary Fig. 3B). There were not significant levels of either PC or PE with medium chain fatty acids (MCFA, carbon between 6 and 12) in the data we obtained. We next analyzed the distribution of PC and PE phospholipid species assigned by the combined number of double bonds present in both FA chains to represent their oxidation state. Interestingly, we observed that BRQ treatment resulted in a significant shift towards increased oxidation of lipid chains in PC (Fig. 3F), but to a much smaller degree in PE (Fig. 3G). Further analysis showed that BRQ treatment led to an increase in the total level of poly-unsaturated fatty acid (PUFA, > 1 double bond number in a single fatty acid)-containing PCs and a decrease in saturated and mono-unsaturated fatty acid (MUFA)-containing PC (Fig. 3H). Unlike PC, most PE species in control cells contain PUFA rather than MUFA and saturated FA chains, and the changes in PUFA-containing PEs upon BRQ treatment were significantly less than seen for PUFA-containing PCs (Fig. 3H). PUFA chains in phospholipids facilitate ferroptosis by their ability to propagate lipid peroxidation to adjacent PUFAs within the plane of the membrane[26,27]. Furthermore, we found that DHODH KO in D4M cells also resulted in a similar significant increase in the oxidation of fatty acid chains of PC lipids (Supplementary Fig. 3C–E). These results revealed that the increase in lipid peroxidization induced by DHODH inhibition occurred mostly due to the increase in very long chain, poly-unsaturated fatty acids within the pool of PC lipids.

### BRQ treatment reduced the levels of CDP-choline, an intermediate in phosphatidylcholine synthesis

To gain a broader understanding of the metabolic effects of DHODH inhibition that might inform these alterations in lipid profiles, we next carried out LC-MS based polar metabolite profiling studies in D4M and M14 melanoma cells treated with BRQ. We confirmed that BRQ treatment resulted in significantly increased dihydro-orotate levels and decreased levels of orotate and dependent pyrimidine species (Fig. 3I and Supplementary Fig. 3F–G). We also found that the levels of several UDP-containing metabolites, such as UDP-N-acetylglucosamine (UDP-GlcNAc) and UDP-Glucose, were significantly reduced. Intriguingly, CDP-choline was also dramatically reduced following BRQ treatment (Fig. 3J). This is likely due to reduction in the levels of CTP, which is produced by direct amination of UTP by CTP synthase (Fig. 3K). Similar decreases in CTP and CDP-choline levels were also observed in MC38 and A375 cells upon DHODH KO (Supplementary Fig. 3H–I). However, BRQ treatment did not lead to significant changes in CDP-choline level in A375 cells with DHODH knockdown, suggesting that the reduction of CDP-choline by BRQ is dependent on DHODH (Supplementary Fig. 3I). CTP can be subsequently reacted with phosphocholine to produce the high-energy donor CDP-choline, which is essential to produce PC via the Kennedy pathway, one of the two PC synthesis pathways, with the other being the phospholipid methylation pathway[28] (Fig. 3K). While the Kennedy pathway uses CDP-choline for phosphatidylcholine for direct headgroup addition, the phospholipid methylation pathway produces PC from PE via three sequential methylation reactions mediated by phosphatidylethanolamine N-methyltransferase (PEMT) (Fig. 3K). In contrast to CDP-choline, the levels of CDP-ethanolamine remained unaltered following DHODH inhibition suggesting that PC synthesis would be mostly dependent on the PE methylation by PEMT upon DHODH inactivation. Interestingly, these two pathways are known to generate species of PC that differ in their FA composition. The Kennedy pathway yields PC species with shorter and saturated chains, whereas the phospholipid methylation pathway synthesizes PC species with longer, poly-unsaturated chains[28]. The observed reduction of CDP-choline level upon DHODH inhibition would therefore be expected to lead to a shift in the balance of these two PC synthesis pathways towards the PE methylation pathway, leading to increased synthesis of longer chain, more oxidized PC species, which is exactly what we observed from the metabolomic and lipidomic analysis (Fig. 3C, E, F and H).

### Supplementation of CDP-choline reverses DHODH inhibition-induced alterations in PC metabolism

To test whether CDP-choline plays a critical role in mediating the effects of DHODH inhibition on phospholipid metabolism, we carried out further lipidomic analysis of cells subjected to BRQ inhibition of DHODH with concomitant CDP-choline supplementation with a focus on any effects on PUFA-containing PC. CDP-choline had minimum effects on the overall composition of cellular phospholipids based on the total masses of various major phospholipid classes, including PC and PE (Supplementary Fig. 4A). We analyzed the effect of CDP-choline co-treatment with BRQ on the distribution of PC and PE species with increasing numbers of total double bonds in both lipid tails. As shown in Fig. 4A, supplementing BRQ treated cells with CDP-choline significantly reduced the levels of PCs with high number double bonds, such as those with 4, 5 or 9 and more double bonds total summed in both FA chains. This was reflected in a partial reversal of the decreased MUFA and the increased PUFA containing PC described earlier in response to BRQ treatment (Fig. 4C). Consistent with the minor effects of BRQ on PE (Fig. 3G), only nominal effects of CDP-choline were observed on PE with high number double bonds (Fig. 4B). Significantly, CDP-choline supplementation did not affect the uridine containing nucleotide species caused by BRQ treatment suggesting that these changes in PC lipids were specific to CDP-choline replacement (Supplementary Fig. 4B). These findings demonstrate that DHODH inhibition reprograms PC synthesis via reducing CDP-choline levels.

We next asked whether there were specific subsets of lipid species within the PC population that were both specifically increased in response to BRQ and whose levels were rescued by CDP-choline. We first performed volcano plot analysis on PUFA containing PC lipids to identify lipids whose levels were specifically increased by BRQ (Supplementary Fig. 4C). Further comparison of the abundance of all the 40

https://doi.org/10.1038/s41467-025-59307-y

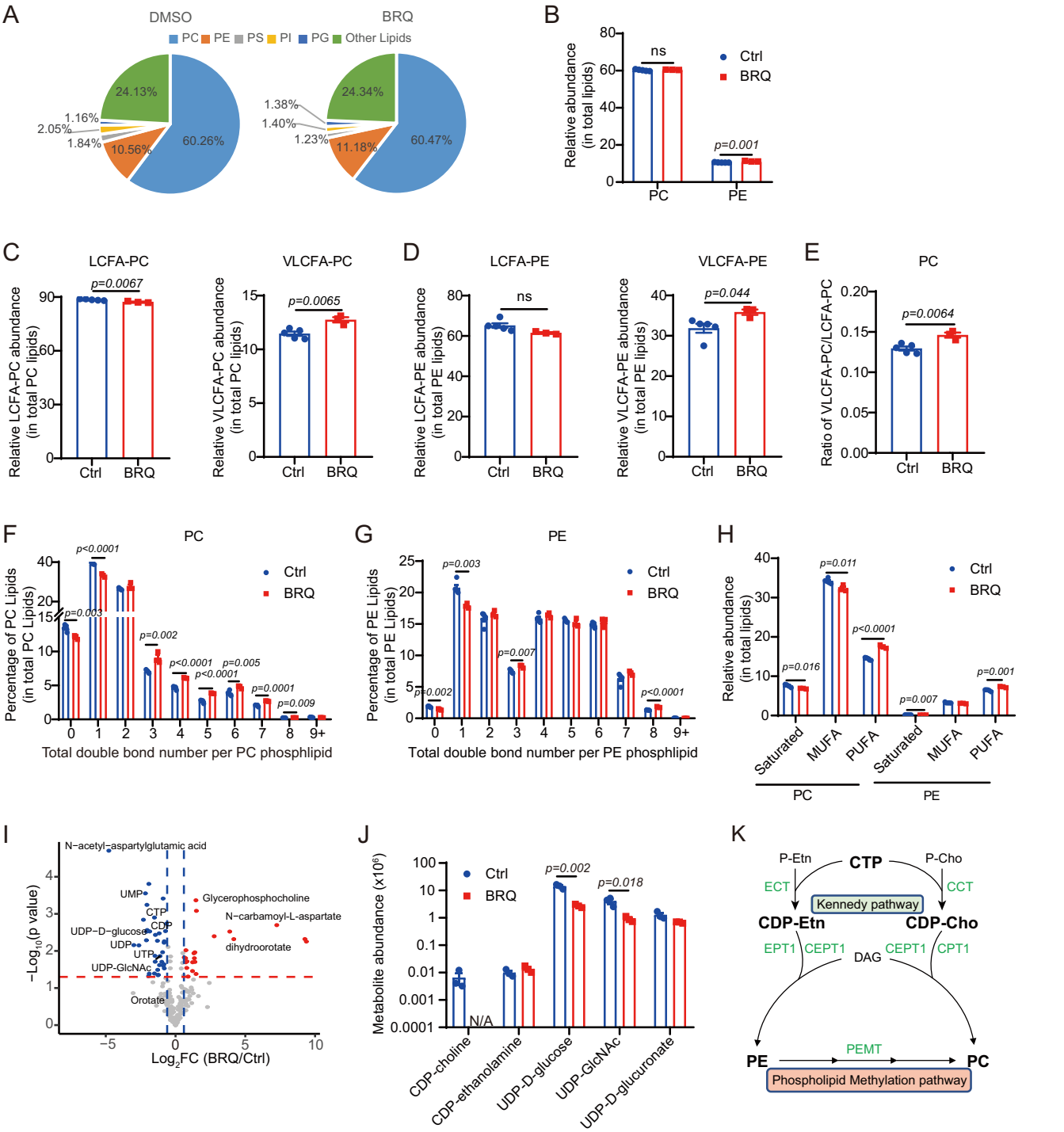


**Fig. 3 | DHODH inhibitor treatment alters phospholipid metabolism and reduces CDP-Choline levels.** Non-polar lipids were extracted from D4M cells treated for 24 h with either DMSO or 1 μM BRQ and subjected to LC/MS (ctrl, $n = 5$; BRQ, $n = 3$, biologically independent samples). **A** BRQ treatment did not lead to major alterations in the relative distribution of among the major classes of cellular phospholipid content. **B** BRQ treatment resulted in no effect on bulk PC lipid content but an increase in PE lipids in D4M cells. **C**–**E** BRQ treatment decreased the relative abundance of LCFA-PC, while increased which of VLCFA in both PC (**C**) and PE (**D**) pools, affecting the VLCFA/LCFA ratios (**E**). **F**, **G** Analysis of the PC (**F**) and PE (**G**) lipid subpopulations defined by the total oxidation summed between their constituent fatty acid chains showed a selective increase in mass of PC lipids containing greater than 3 total double bonds was observed. **H** Examination of saturated, MUFA, and PUFA PC-lipid species showed steady state levels decreased in saturated and MUFA fatty acid chains but an increase in PUFA containing lipids. There was little change in corresponding PE Lipids. (**I**) Volcano plot analysis of polar metabolites from M14 cells treated with 10 μM BRQ. Significant alterations in metabolites related to pyrimidine synthesis were observed ($n = 3$ biologically independent samples). **J** Quantification of selected uridine-derived metabolites upon BRQ treatment ($n = 3$ biologically independent samples). **K** Diagram of PE and PC Kennedy pathway synthesis the role of PEMT mediated phospholipid methylation for PC production. For all panels, $p$ values were calculated by unpaired two-tailed Student's t-tests. Data are represented as mean ± SEM. Source data are provided as a Source Data file.

https://doi.org/10.1038/s41467-025-59307-y

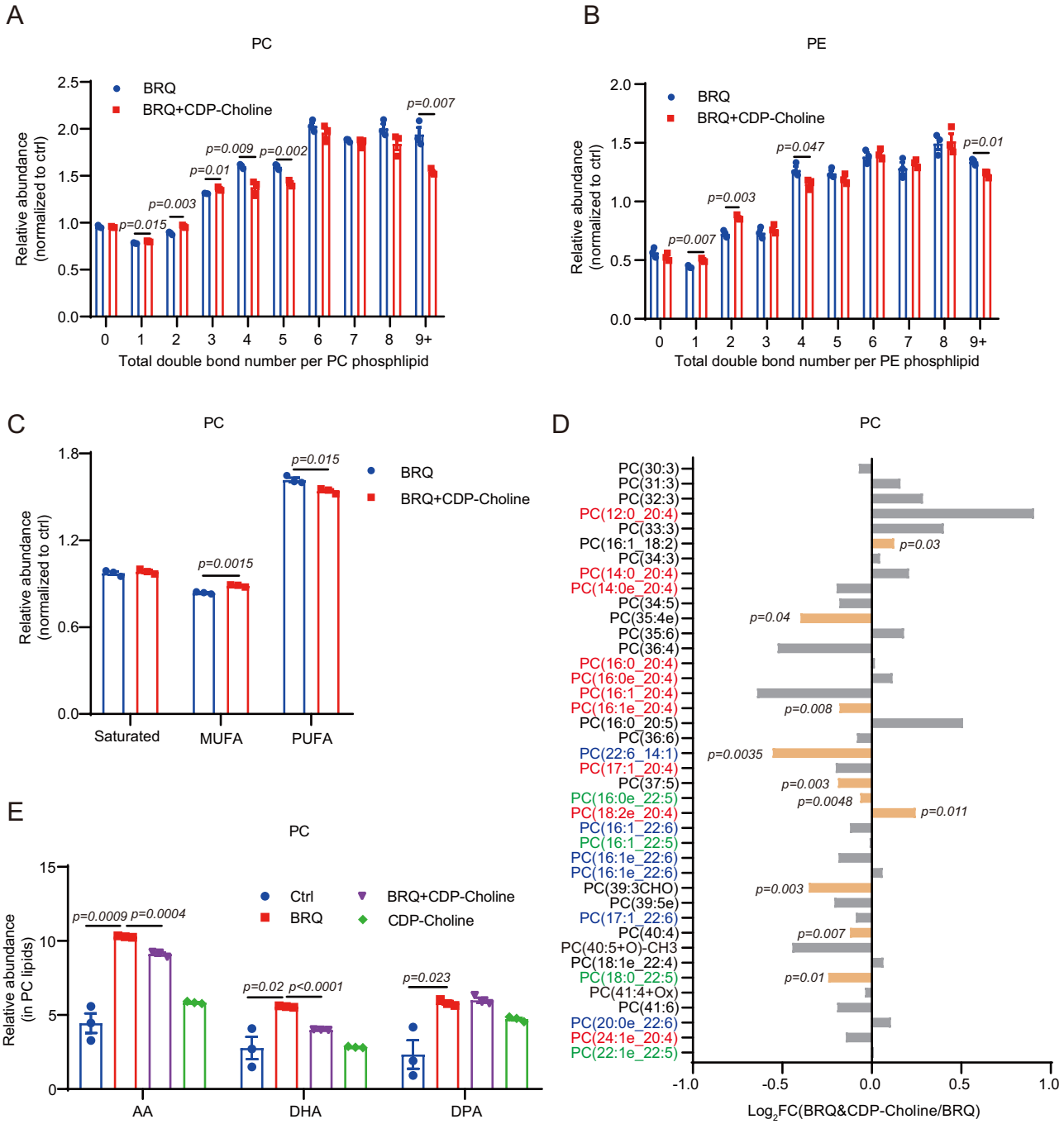


**Fig. 4 | Supplementation of CDP-Choline reverses DHODH inhibition-induced alterations in phospholipid metabolism.** D4M cells were treated with DMSO, 1 μM BRQ, 300 μM CDP-Choline, or BRQ with CDP-Choline for 24 h and lipids were extracted and subjected to LC/MS for lipid identification ($n = 3$ biologically independent samples). **A**, **B** Analysis of the PC (**A**) and PE (**B**) lipid subpopulations defined by the total oxidation summed between their constituent fatty acid chains showed a selective decrease in mass of PC lipids containing greater than 3 total double bonds upon CDP-choline supplementation of BRQ treated cells relative to that from cells that were BRQ treated alone. **C** Effects of CDP-choline supplementation of BRQ treated cells examining saturated, MUFA and PUFA PC lipids. **D** Analysis of the effect of CDP-choline supplementation on specific PC lipids increased upon BRQ treatment alone. Orange bars represent lipid species with significant changes. Different colors of Y-axis labels represent different lipid subgroups: Red represents AA, green represents DPA, and blue represents DHA. **E** Effects of BRQ and CDP-choline supplementation on relative concentrations of PC lipids containing AA, DPA, and DHA fatty acids. Data for panels **A**–**C** were normalized to the control group. *p* values were calculated by two-tailed unpaired Student's t-tests. Data are represented as mean ± SEM. Source data are provided as a Source Data file.

PUFA-containing PC species increased in D4M cells treated with BRQ in cells treated with BRQ supplemented with CDP-choline showed that 10 of them exhibited significant changes upon CDP-choline supplementation, with 8 of them being partially rescued by CDP-choline (Fig. 4D). Many of the lipids that exhibited increases in these analyses were arachidonic acid (AA, 20:4), docosapentaenoic acid (DPA, 22:5), and docosahexaenoic acid (DHA, 22:6) lipids. AA, DPA, and DHA (Supplementary Fig. 4C and Fig. 4D) contain bis-allylic bridging single bonds that intersperse their double cis-bonds creating reactive centers for the propagation of lipid peroxidation that facilitate ferroptosis[26].

This prompted us to examine the total levels of all AA-, DPA-, and DHA-containing PC lipids upon treatment with BRQ and CDP-choline. Indeed, the levels of these lipid classes were all increased in response to BRQ, and CDP-choline addition partially rescued the effects of BRQ on AA- and DHA- PC lipids, but not the DPA-PC lipids (Fig. 4E). Examination of comparable PE lipids showed no significant increases in response to BRQ (Supplementary Fig. 4D). These findings further support that CDP-choline metabolism plays a critical role in DHODHi-induced ferroptosis by increasing the levels of PUFA-containing (such as AA and DHA) PC populations, which are major contributors to membrane lipid peroxidation[26].

### CDP-choline supplementation reverses DHODH inhibition-induced ferroptosis and sensitization to T cell cytotoxicity

We next examined whether the reduced CDP-choline level and its subsequent impact on the synthesis of various PC species contributed to the effect of DHODH inhibition on ferroptosis induction. We found that CDP-choline supplementation was able to reverse the effects of both DHODH inhibitors (BRQ and BAY2402234) and DHDOH KO on inducing lipid peroxidation (Fig. 5A–C and Supplementary Fig. 9E), but not lipid peroxidation induced by the GPX4 inhibitor RSL-3 (Fig. 5A). Accordingly, in contrast to BRQ-induced, RSL-3-induced ferroptotic cell death in D4M cells was not reversed by CDP-choline supplementation (Supplementary Fig. 5A and 9F). In addition, inhibition of the phospholipid methylation pathway by knocking down PEMT (Supplementary Fig. 5B) also abated BRQ-induced increases in lipid peroxidation in D4M cells (Supplementary Fig. 5C and 5J, K), suggesting that a dynamic interplay between the CDP-choline-dependent Kennedy pathway and the phospholipid methylation pathway is critical for DHODH inhibition induced ferroptosis. As a positive control, uridine supplementation completely reversed the effects of BRQ on lipid peroxidation in D4M cells (Supplementary Fig. 5E). Importantly, we found that CDP-choline also reversed the further increase in lipid peroxidation in cancer cells upon $CD8^+$ T cell exposure on top of DHODH inhibition (Fig. 5D, E and Supplementary Fig. 5D).

We further asked whether CDP-choline supplementation concomitant to BRQ treatment would affect the susceptibility of cancer cells to $CD8^+$ T cell-mediated killing described earlier. Supplementation of various cancer cells with CDP-choline during BRQ or BAY2402234 treatment rescued the BRQ-induced or BAY2402234-induced enhanced killing of cancer cells by $CD8^+$ T cells (Fig. 5F–H and Supplementary Fig. 5F). CDP-choline also reduced the ability of BRQ treated cancer cells to induce increases in IFNγ expressing $CD8^+$ T cells. (Fig. 5I), consistent with CDP-choline reversing of the mechanism by which BRQ drives $CD8^+$ T cell cytotoxicity towards the treated cells. Importantly, blocking the phospholipid methylation pathway by *Pemt* shRNA knockdown also attenuated the ability of BRQ to promote killing of D4M cells by T cells (Fig. 5J). Consistent with our observation on the increases in levels of AA and DHA-containing PCs upon DHODH inhibition (Fig. 4E), AA and DHA fatty acids were recently shown to induce tumor cell ferroptosis in YUMM5.3 melanoma cells either by themselves or in combination with IFNγ treatment[29]. Interestingly, we found that treatment of D4M cells with either AA or DHA, but not DPA, also led to enhanced $CD8^+$ T cell mediated killing of tumor cells, which were reversed by CDP-choline supplementation (Supplementary Fig. 5G). These findings together support that CDP-choline-dependent phospholipid metabolism plays a critical role in mediating the regulation of ferroptosis and immune evasion by DHODH in cancer cells.

### Inactivation of DHODH in cancer cells enhances the anti-tumor activity of PD-1 blockade in mouse models

Given our observation that DHODH inhibition increased susceptibility of tumor cells to $CD8^+$ T cell killing in vitro, we sought to assess whether BRQ may enhance the efficacy of anti-PD-1 checkpoint blockade in syngeneic transplantable mouse tumor models. Six-week-old C57BL/6 J mice were used for allograft tumor implantation of D4M-UV3 mouse melanoma cells, which were derived from D4M cells with UV exposure to increase tumor mutational burden and hence sensitivity to immune checkpoint blockade[30]. Once tumors reached 120-180 $mm^3$ mice were randomly assigned to four groups and administered either 100 µg of rat IgG2a isotype control or rat anti-mouse-PD-1 antibody by intraperitoneal injections, BRQ together with either IgG isotype control or anti-PD-1 antibody every other day (Supplementary Fig. 6A). To minimize potential off-target effects, we use a very low dose (1.25 mg/kg) of BRQ than those in recent mouse studies (25-50 mg/kg)[7,12,16]. We found that, although treatment with this low dose BRQ alone did not significantly affect tumor growth, the combination of this low dose BRQ and anti-PD-1 antibody significantly inhibited tumor growth compared to either treatment alone (Fig. 6A and Supplementary Fig. 6B).

Next, we examined whether genetic ablation of *Dhodh* in cancer cells is sufficient to sensitize tumors to anti-PD-1 treatment. Mice bearing D4M DHODH KO tumors or WT control tumors were treated with either anti-PD-1 or isotype control IgG. As in previously reported data[30], anti-PD-1 treatment did not significantly reduce D4M WT tumor growth, probably due to the low mutation burden; however, anti-PD-1 treatment significantly decreased the growth of the D4M DHODH KO tumors (Fig. 6B and Supplementary Fig. 6C). Flow cytometry analyses revealed that while anti-PD-1 treatment promoted small increases in $CD8^+$ T cell infiltration in D4M WT tumors ($p = 0.179$), D4M DHODH KO tumors exhibited significantly higher levels of $CD8^+$ T cells, but not $CD4^+$ T cell infiltrates (Fig. 6C, D). We also observed higher percentages of $IFN\gamma^+$ $CD8^+$ T cells in the tumors from DHODH KO cells compared to WT control tumors treated with anti-PD1 or isotype control antibodies (Fig. 6E). We did not observe significant differences in the numbers of PMN- or M- MDSCs among tumors with DHODH KO or WT, treated with or without anti-PD-1 (Supplementary Fig. 6D, E). Immunofluorescence analysis of 4-HNE antibody staining, indicative of lipid peroxidation level, confirmed that tumors from DHODH KO cells exhibited increased lipid peroxidation compared to those from WT cells, whereas anti-PD1 treatment did not have any significant impact on 4-HNE staining by itself or in combination with BRQ treatment (Fig. 6F, G and Supplementary Fig. 6F). Likewise, we also observed higher levels of COX-2 staining in DHODH KO tumors compared to DHODH WT tumors (Supplementary Fig. 6G). RNAseq analysis of these D4M tumor samples from various treatment groups of mice revealed higher scores of cytotoxic T lymphocyte (CTL), T cell receptor signaling and interferon alpha and gamma response signature in tumors from the BRQ treated animals (Fig. 6H and Supplementary Fig. 6H, I). Lastly, to investigate the clinical implications of our findings, we carried out spatial transcriptomic analysis using a public dataset of human melanoma metastasis specimens[31]. After assigning discrete cell types using Robust Cell Type Decomposition (RCTD), we uncovered an inverse relationship between DHODH levels in tumor cells and the average distance between T cells and tumor cells in melanoma patient ($p = 0.0003$, Student's *t*-test) (Fig. 6I, J). We also performed spatial transcriptomic analysis on two public datasets of intestinal and ovarian tumors from patients[32]. Through spatial segmentation of regions with high versus low *DHODH* expression, again we found an inverse relationship between *Dhodh* mRNA levels and T cell infiltration and activation status (Supplementary Fig. 7). Taken together, our findings support a key role of DHODH in the evasion of cancer cell from CTL-mediated immune elimination in vivo.

## Discussion

Our current study establishes DHODH as a key metabolic regulator of tumor immune evasion. We demonstrated inhibition of DHODH in tumor cells by either pharmacological or genetic approaches promoted lipid peroxidation, which made them more susceptible to $CD8^+$

https://doi.org/10.1038/s41467-025-59307-y

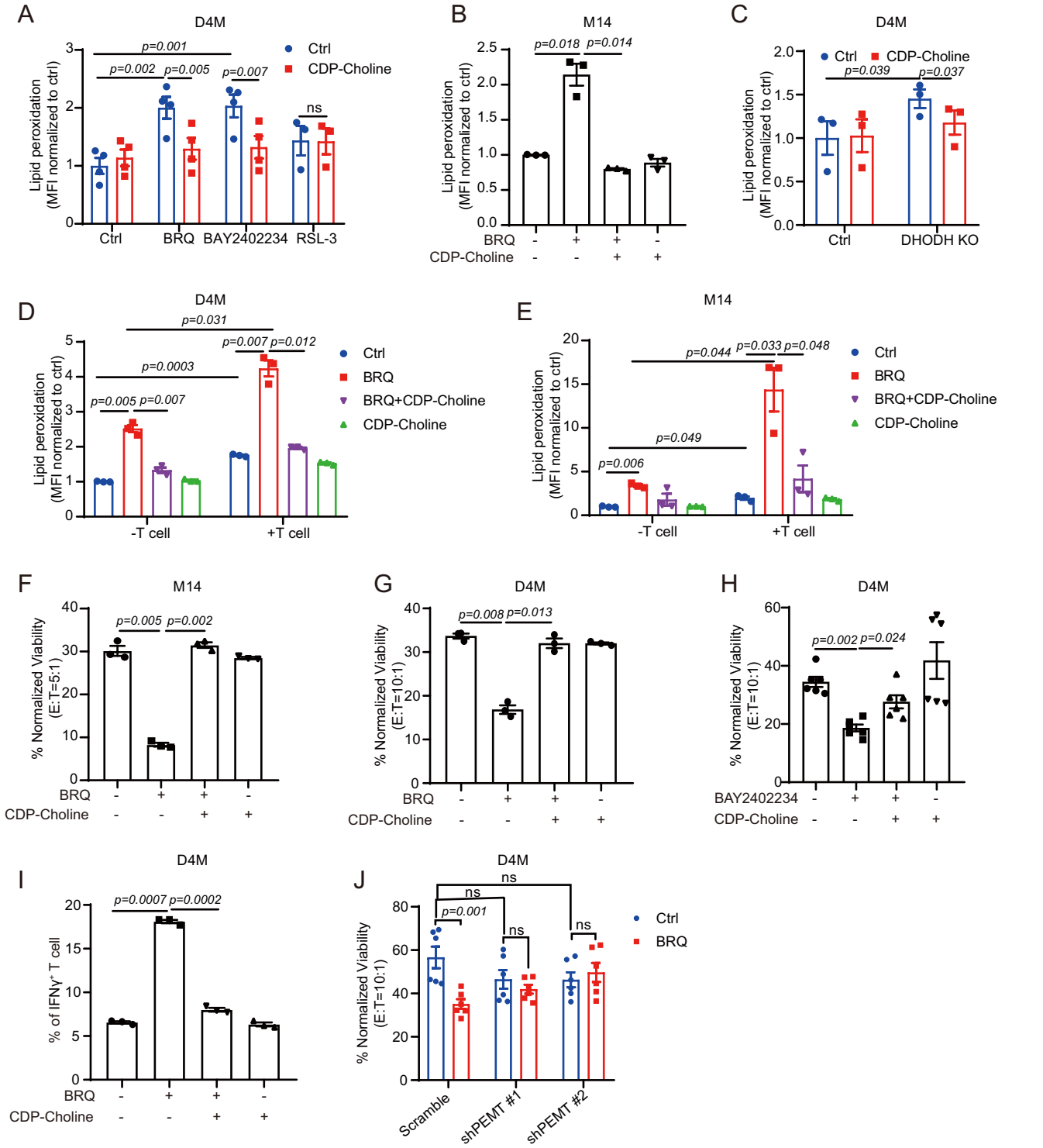


T cell mediated killing through ferroptotic cell death (Fig. 6K). Emerging evidence indicates a critical role of tumor cell ferroptosis in regulating tumor immune evasion. Wang et al. recently reported that ferroptotic cell death of tumor cells is implicated in the cytotoxicity exerted by immunotherapy activated $CD8^+$ T cells[24]. They showed that IFNγ secreted by $CD8^+$ T cells downregulated the expression of the cystine/glutamate antiporter system $xc^-$, a key component of ferroptosis machinery, leading to reduced GPX4 activity and enhanced lipid peroxidation[24]. In addition, ferroptotic cells could also promote release of damage-associated molecular patterns (DAMPs), which would further induce immunologic cell death and potentiate antitumor immunity[33–36]. Consistent with this notion, we found higher levels of $CD8^+$ T cell infiltration in DHODH KO tumors than those in WT tumors (Fig. 1C). It is notable that BRQ was recently found to increase cell surface MHC class I expression[37] in cancer cells. We also observed increased H2-Kb expression (~4 folds) in D4M cells upon BRQ treatment, while only a slight increase (~1.3 folds) in *Dhodh* knockout cells (Supplementary Fig. 2H and I). However, these changes appear to be independent of ferroptosis, since co-treatment of ferrostatin-1 failed to reverse the effects of BRQ or DHODH KO on H2-Kb surface expression (Supplementary Fig. 2H and I). Our findings here establish a previously unappreciated role of DHODH in regulating tumor cell evasion via

**Fig. 5 | Supplementation of CDP-Choline reverses DHODH inhibition-induced ferroptosis and sensitization of T cell cytotoxicity. A** Increased lipid peroxidation in D4M cells observed with 24 h 1 μM BRQ and 10 nM BAY2402234 treatment was reversed with 300 μM CDP-Choline supplementation but not in 1 μM RSL-3 treated cells, ($n = 4$ for ctrl, BRQ and BAY2402234 group; $n = 3$ for RSL-3 group, biologically independent experiments). **B** Lipid peroxidation in M14 cells treated with 1 μM BRQ ($n = 3$ biologically independent experiments) and (**C**) DHODH KO in DM4 cells was also reversed by 300 μM CDP-Choline ($n = 3$ biologically independent experiments). **D** CDP-Choline reverses BRQ-induced lipid peroxidation both in the presence and absence of activated CD3/CD28-activated $CD8^+$ T cells. Data were normalized to parallel DMSO-treated D4M cells without $CD8^+$ T cell co-culture ($n = 3$ biologically independent experiments). **E** Lipid peroxidation in M14 cells pre-treated as in (**D**) in the presence or absence of $CD8^+$ T cell co-culture for 48 h ($n = 3$ biologically independent experiments). CDP-choline supplementation reduces the cytotoxic effects of $CD8^+$ T cell on (**F**) M14 and (**G**) D4M cells pre-treated with DMSO or 1 μM BRQ with or without 300 μM CDP-Choline for 48 h. Cells were co-cultured with activated human $CD8^+$ T cells at 5:1 E:T or 10:1 ratio, respectively for 48 h ($n = 3$ biologically independent experiments). **H** Increased cytotoxic of $CD8^+$ T cell activity towards D4M pre-treated with 10 nM BAY2402234 was also mitigated with 300 μM CDP-Choline for 24 h. Data were normalized to parallel cultures treated in the absence of $CD8^+$ T cells ($n = 6$ biologically independent experiments). **I** BRQ-driven increase in IFNγ expression by mouse $CD8^+$ T cells co-cultured with pre-treated D4M cells was reduced with CDP-choline supplementation ($n = 3$ biologically independent experiments). **J** *Pemt* knockdown in D4M cells mitigated the BRQ-induced increase in their $CD8^+$ T cell-directed killing. D4M of the indicated genotype were pre-treated with DMSO or 1 μM BRQ followed by co-culture with CD3/CD28-activated murine T cells ($n = 6$ biologically independent experiments). For all panels, $p$ values were calculated by paired two-tailed Student's t-tests. Data are represented as mean ± SEM. Source data are provided as a Source Data file.

maintenance of CDP-choline homeostatic synthesis of PC and demonstrate that ferroptosis induced by DHODH inhibition sensitizes cancer cells to $CD8^+$ T cell mediated killing and further potentiates IFNγ expression in $CD8^+$ T cells. Deranged DHODH activity and CDP-choline homeostasis could act as signals for defective cells and operate in a protective mechanism against ferroptosis-induced cell clearance by the immune system. Since there are various other chemotherapy agents targeting pyrimidine synthesis, it would be interesting to explore whether they have similar effects as DHODH inhibitors on phospholipid metabolism and immune evasion of cancer cells.

While the roles of DHODH in nucleotide metabolism and hence cell proliferation control are well established, its connection to ferroptosis was not revealed until recently and whether DHODH is a major contributor to ferroptosis regulation remains controversial[20,38,39]. To catalyze the conversion of dihydroorotate to orotate, DHODH uses flavin mononucleotide (FMN) as a cofactor and transfer electrons to mitochondrial CoQ10 (coenzyme Q10, ubiquinone), generating ubiquinol, a radical-trapping antioxidant, in a redox-dependent reaction. This reduction of mitochondrial CoQ10 to ubiquinol was recently suggested to mediate the effect of DHODH inactivation on induction of lipid peroxidation and ferroptotic cell death in cancer cells with low GPX4 expression[20]. Findings from our studies here confirm the effects of DHODH inactivation on inducing ferroptosis and further reveal decreased CDP-Choline level upon DHODH inactivation significantly contributed to the underlying the molecular mechanism. Of note, in contrast to the relatively higher concentration of BRQ (500 μM) used to induced CoQ10-dependent lipid peroxidation and ferroptosis in cancer cells by Mao et al. and others[20,40], 1 μM of BRQ or 10 nM BAY2402234 were sufficient to induce CDP-choline-reversable lipid peroxidation and ferroptosis in our studies (Fig. 5A, B and Supplementary Fig. 5A). In addition, pre-treatment of D4M melanoma cells with 4-CBA to inhibit CoQ synthesis did not significantly reverse the effects of either BRQ or BAY2402234 in sensitizing them to killing by $CD8^+$ T cells (Supplementary Fig. 2J). Furthermore, we also observed that supplementing $MitoQH_2$ in D4M *Dhodh* KO cells did not significantly change the sensitivity of cells to $CD8^+$ T cell-mediated killing (Supplementary Fig. 2K). These findings suggest that the CDP-choline dependent mechanism could be distinct from the CoQ10 dependent mechanism.

Our findings here reveal a previously under-appreciated role of DHODH in regulating PC homeostasis resulting in increased levels or PUFA-containing PC. DHODH, via modulating CDP-choline levels, plays a key role in regulating the balance of the Kennedy versus the phospholipid methylation pathway of PC synthesis (Fig. 3K), and consequently increased the incorporation of PUFA into PC, which constitutes the most abundant phospholipid species in the cell. Consistent with this model, we found that either supplementation of CDP-choline to restore the Kennedy pathway or inhibition of the phospholipid methylation pathway by knocking down PEMT rescued the effects of DHODH inhibition on inducing lipid peroxidation and increasing susceptibility to $CD8^+$ T cell cytotoxicity (Fig. 5A–C, F–J and Supplementary Fig. 5C). The Kennedy and phospholipid methylation pathways generate PC with different levels of FA chain oxidation due to differences in diacyl glycerate substrate specificities of their biosynthetic enzymes (Fig. 3K). Choline phosphotransferase 1 (CPT1) produces only PC by direct utilization of CDP-choline and prefers saturated DAG with chains of 16 and 18 carbons[41]. The dual-specificity choline/ethanolamine phosphotransferase 1 (CEPT1) is responsible for the remaining PC and also contributes to PE production. In contrast to CPT1, CEPT1 readily utilizes DAGs with longer, unsaturated fatty acid chains, such as AA, DHA, and DPA[41]. Indeed, when PC synthesis was isotopically traced using differentially labeled CDP-choline and CDP-ethanolamine, it was determined that PC originating from PE through the phospholipid methylation pathway possessed significantly higher incorporation of very long chain PUFA[28], consistent with our observations in cells treated with BRQ (Fig. 3C and F). We did not detect significant differences in the PUFA content in DAG, suggesting that the increase in PUFA-containing PC was not due to an increase in DAG-PUFA availability (Supplementary Fig. 3J). Therefore, the reduction in CDP-choline, due to the reduction in CTP upon DHODH inhibition, best explains this mechanistic shift in PC synthesis, which was confirmed by the phenotypic rescue upon CDP-choline supplementation (Fig. 4A and C). It is noteworthy that we found a marked reduction in CDP-choline but not in CDP-ethanolamine upon DHODH inhibition (Fig. 3J). This discrepancy can be explained by differences in the affinities for CTP of mammalian CTP: phosphocholine cytidylyltransferase (CCT) and CTP: phosphoethanolamine cytidylyltransferase (ECT) (Fig. 3K), which have Km for CTP of 1.4-4 mM[21] and 48-102 μM[42,43], respectively, thus favoring CDP-ethanolamine production under low CTP conditions. Further characterization of this intricate and under-studied regulatory network of phospholipid synthesis (Fig. 3K) may provide additional mechanistic insight into how immune evasion of cancer cells is regulated by phospholipid metabolism, beyond DHODH and CDP-choline. On the other hand, whether the effects of DHODH inhibition on CDP-choline and phospholipid metabolism could contribute to other known biological activities of DHODH inhibitors, such as transcriptional elongation[6], DNA damage response[44], myeloid cell differentiation[7], erythropoiesis[45] and antigen presentation[37], deserves future investigations.

DHODH is a promising therapeutical target in cancers as demonstrated in numerous preclinical cancer models[6–14]. The DHODH inhibitor BRQ has been evaluated in several Phase I clinical trials for various cancers[46,47]. However, its clinical development was discontinued due to the narrow therapeutic window and lack of efficacy in solid tumors[48,49]. Several new generations of DHODH inhibitors (i.e., BAY2402234, JNJ-74856665 and AG-636)[21,50,51] with greater potency and better selectivity have recently been developed for hematological

https://doi.org/10.1038/s41467-025-59307-y

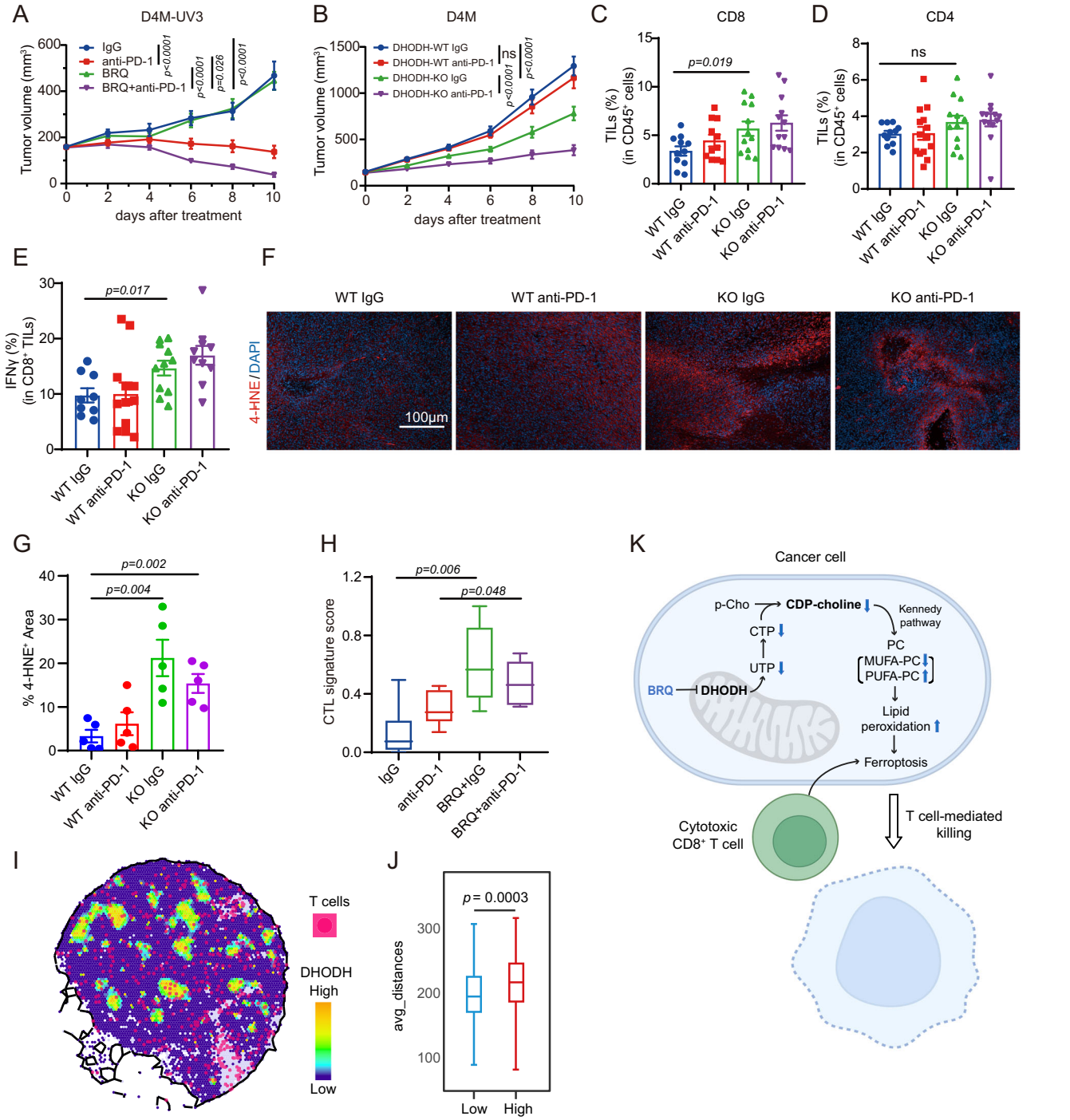


**Fig. 6 | Inactivation of DHODH in cancer cells enhance the anti-tumor activity of PD-1 blockade in mouse models. A** Effects of BRQ combined with anti-PD-1 treatment on the growth of D4M-UV3 tumors in C57BL/6 mice. ($n = 7$ mice for each group). **B** Effects of anti-PD-1 and IgG control treatments on the growth of DHODH-expressing versus DHODH KO D4M tumors in C57BL/6 mice. ($n = 13$ mice for DHODH KO anti-PD-1 group, $n = 11$ mice for other groups). **C** Analysis of tumor-infiltrating T cells revealed a significant increase in $CD8^+$ T cells in DHODH-deficient D4M tumors ($n = 11$ mice each group). **D** Analysis of tumor-infiltrating $CD4^+$ T cells revealed a similar representation in DHODH-expressing and DHODH KO D4M tumors ($n = 11$ mice each group). **E** Infiltrating $CD8^+$ T cells isolated from DHODH KO tumors exhibited increased INFγ expression, compared to those from DHODH WT tumors ($n = 9$ mice for each group) (**F**) Immunofluorescence analysis of tumors from various treatment groups from (**B**) with 4-HNE antibody. **G** Quantification of 4-HNE staining ($n = 5$ each condition). **H** Cytotoxic T Lymphocyte (CTL) signature score analysis of RNASeq data obtained from various groups of D4M tumors ($n = 6$ for each group). **I** Spatial expression pattern of DHODH in tumor cells and T cell in human melanoma metastasis specimens. **J** Average distances of T cell to tumor cells with high or low DHODH levels as presented in panel **I**. Data are presented with median values shown in boxplots, where the lower and upper hinges correspond to 25th and 75th percentiles (**H**) or 10th and 90th percentiles (**J**) of the data. The lower and upper whisker range from minimum to maximum. **K** Schematic diagram of the model on how DHODH regulates tumor cell immune evasion. The cell icons were created in BioRender[62]. For panels **A**, **B**, the adjusted $p$ values were calculated using a two-sided Tukey's multiple comparisons test. For panels **C**–**E**, **H** and **J**, $p$ values were calculated by unpaired two-tailed Student's t-tests. For panel **G**, $p$ values were calculated using original one-way ANOVA test. Data are represented as mean ± SEM. Source data are provided as a Source Data file.

malignancies, including acute myeloid leukemia, myelodysplastic syndrome, multiple myeloma, and lymphoma, but their potential applications as new therapeutics for solid tumors are not clear. Interestingly, in the current study, we found that a low dosage of BRQ (1.25 mg/kg), which had no detectable efficacy against tumor growth on its own, greatly enhanced the response to anti-PD1 therapy in mice (Fig. 6A). Further, knockout of *dhodh* in cancer cells also resulted in improved sensitivity to anti-PD-1 therapy in the anti-PD-1-resistant D4M model (Fig. 6B). These findings on the role of DHODH in regulating tumor immune evasion and the effect of BRQ on enhancing the response to anti-PD-1 immune checkpoint blockade therapy in mice suggest that combining DHODH inhibitors with immune checkpoint blockade, and potential other immunotherapies, represents a path forward for the development of these drugs against solid tumors and therefore warrants future translational investigations.

It must be kept in mind that in addition to targeting tumor cells and enhancing anti-tumor immunity, pharmacological inhibitors of DHODH are expected to exert pleiotropic effects on other types of cells as well. Leflunomide, a DHODH inhibitor used to treat rheumatoid arthritis and multiple sclerosis, is known to suppress T cell responses in the autoimmunity settings[52]. More recently, leflunomide was shown to block the early phase of T cell expansion in a narrow time window during infection, but not the memory T cell development in Listeria monocytogenes and lymphocytic choriomeningitis virus infection models[53]. Moreover, BRQ was recently found to inhibit the biogenesis of myeloid-derived suppressor cells, a major group of immune suppressive cells in the tumor microenvironment, from early-stage myeloid progenitors[54], suggesting that inhibition of DHODH in MDSCs would also enhance anti-tumor immunity. Hence, when considering the therapeutical effects of DHODH inhibitors in cancer, it is important to take the relative contributions of their effects on different cell types in the tumor microenvironment into account in a systematic fashion. Pyrimidine synthesis is an essential metabolic pathway for cell growth and proliferation. In addition to the de novo pyrimidine synthesis from glucose and amino acids that DHODH participates in, pyrimidines are also recycled by the savage pathway that utilizes extracellular nucleosides and nucleotide bases or intracellular nucleic acids derived from DNA/RNA degradation. Therefore, the relative contribution of the de novo versus the savage pathways is expected to dedicate the sensitivity of different types of cells to DHODH inhibition. Lastly, off-target effects of various DHODH inhibitors have been documented[55,56]. Therefore, in addition to the pharmacologic approach, genetic deletion or inactivation of DHODH in various non-tumor cell types, including T cells and MDSCs, are required to further elucidate its function in anti-tumor immunity in future studies.

## Methods

### Mouse studies

For allograft models, 6 ~ 8 weeks old female C57BL/6 mice were injected subcutaneously in the right flank with D4M (D4M-3A)[15], YUMMER1.7 or MC38 mouse cells (0.5 million cells per mouse). Once tumor sizes reached 120–180 $mm^3$, animals were randomly assigned to two groups that were administered Brequinar (BRQ) (TOCRIS, no.6196) at the dose indicated or DMSO via Intraperitoneal injection every other day. D4M DHODH WT-hygro (WT) and D4M DHODH KO-hygro (KO) cells were injected subcutaneously on C57BL/6 or NOD.Cg-Prkdcscid Il2rgtm1Wjl/SzJ (NSG) mice. C57BL/6 and NSG mice (stock no.005557) were purchased from Taconic Farms and Jackson Laboratory, respectively. For Fer-1 treatment experiment, once tumor reached 80-120 $mm^3$, animals were randomly assigned to two groups that were administered 5 mg/kg of Fer-1 or DMSO via intraperitoneal injection every other day. For anti-PD-1 treatment experiment, once tumor sizes reached 120–180 $mm^3$, animals were randomly assigned to the four groups that were administered 100 μg of anti-PD-1 or IgG isotype control via Intraperitoneal injection every other day. Tumor dimensions were calculated from caliper measurements by using the following formula: (length × $width^2$)/2. All mice were bred and housed under specific-pathogen-free conditions with 12-h dark/light cycle under 21 ± 1 °C temperature and 55–60% humidity and provided ad libitum access to water and food. All animal experiments were conducted in accordance with the Institutional Animal Care and Use Committee guidelines at the Massachusetts General Hospital.

### Cell culture studies

D4M, MC38, MC38-OVA, and ID8 cells stably expressing different gRNA targeting different sequences of DHODH were established by using lentiCRISPRv2 vector and established by hygromycin treatment. The knockout efficiency was validated by examining the DHODH protein expression by Western Blot analysis. The *Dhodh* gRNA#a (GTAGAAATGGTCGTCCCCCG) and gRNA#b (TTGATCCAGAGTCGG CGCAC) stable cell lines were used for further study. pLKO.1-puro-vectors containing shDHODH (TRCN0000025868) were purchased from Sigma and used to establish M14 and A375 stable cell lines. pLKO.1-puro-vectors containing shPEMT#1 (TRCN0000313023) or shPEMT#2 (TRCN0000312024) were purchased from Sigma and used to establish D4M stable cell lines with puromycin selection. D4M, YUMMER1.7, ID8, MC38 and MC38-OVA-zsGreen were cultured in Dulbecco's Modified Eagle Medium (Gibco, no.10313039) supplemented with 10% FBS, 1% penicillin/streptomycin (Gibco, no.15140122) and 1% L-Glutamine (Life Technologies, no.25030081). M14 and A375 were cultured in RPMI 1640 (Gibco, no.21870092). All cells were free of mycoplasma contamination. Cells were cultured at 37 °C with a humidified atmosphere of 5% CO2.

### Cell death assay

Cell death was measured by propidium iodide (Sigma, no. P4864) staining using a flow cytometer. Cells were seeded into 24-well plates at a density of 50% confluence cultured overnight and then treated with various reagents. Total cells, including floating dead cells, were stained with 100 ng/ml propidium iodide, and the propidium iodide-positive cells were analyzed using flow cytometer BD FACSCanto (BD Biosciences).

### T cell isolation and stimulation

Mouse $CD8^+$ T cells were isolated from the spleen of naïve C57/BL6 mice or OT-1 mice (Jackson Laboratory, stock no.003831) with CD8a (Ly-2) MicroBeads (Miltenyi Biotec, no.130-117-044). In brief, single cell suspension was generated by forcing spleens through 70 μm filters, followed by RBC removal by incubation with ACK RBC lysis buffer (Lonza, no. BP10-548E) and washing with PBS. Then cell suspensions were incubated with anti-CD8a microbeads and sorted using MS columns. The magnetically labeled $CD8^+$ T cells were eluted as the positively selected cell fraction. Human $CD8^+$ T cells were isolated from human PBMCs (Zen-Bio Inc, no. SER-PBMC-P-F) with the Naive $CD8^+$ T Cell Isolation Kit (Miltenyi Biotec, no.130-093-244) in a two-step procedure. First, naive T cells were enriched by depletion of non-naive T cells and NK cells, which were indirectly magnetically labeled with a cocktail of biotin-conjugated antibodies and Anti-Biotin MicroBeads. In the second step, the enriched naive T cells were labeled with anti-CD8 MicroBeads for subsequent positive selection of the $CD8^+$ naive T cells. Mouse $CD8^+$ T cells were stimulated with 10 μg/ml anti-CD3 (Invitrogen, no.16-0031-85) and 1 μg/ml anti-CD28 antibodies (Invitrogen, no.16-0281-85). Human $CD8^+$ T cells were stimulated with ImmunoCult™ Human CD3/CD28 T Cell Activator (STEMCELL, no.10971). OT-1 $CD8^+$ T cells from OT-1 mice were stimulated with 1 μg/ml OVA 257-264 (SIINFEKL) peptide (Sigma, no. S7951). T cells were cultured in RPMI-1640 supplemented with 10% FBS, 1% penicillin/streptomycin, 1% L-Glutamine, 200U IL-2 (PeproTech, no. AF2121220UG), and 50 μM 2-mercaptoethanol.

### In Vitro T cell cytotoxicity assay

Tumor cells were pre-treated with drugs for 24 h or 48 h, as indicated, washed with PBS twice to remove drugs, and pre-labeled by CellTrace CFSE dye (Invitrogen, no. C34554) or CellTrace Far Red dye (Invitrogen, no. C34564) and reseeded to 24-well plates. Uridine (no. U3003), Ferrostatin-1 (Fer-1, no. SML0583), Cytidine 5′-diphosphocholine sodium salt hydrate (CDP-Choline, no.30290) were purchased from Sigma. BAY2402234 (no. S8847) was purchased from Selleck Chemicals, PCT299 (no. HY-124593) was purchased from MedChemExpress, and RSL-3 (no.192881), ASLAN003 (no. 33516), Mitoquinol (no. 89950), Arachidonic acid (AA, no. 90010), Docosahexaenoic Acid (DHA, no. 90310) and Docosapentaenoic Acid (DPA, no. 90165) were purchased from Cayman Chemical. $CD8^+$ T cells were activated by anti-CD3/CD28 for 3 days and cultured for 2 additional days. For MC38-OVA killing assay, the OT-1 $CD8^+$ T cells were activated by OVA peptide (1 μg/ml) for 5 days. Prior to $CD8^+$ T cells co-culture, $3 \times 10^4$ pre-treated tumor cells were plated into 24-well plates and cultured overnight, then co-cultured with activated $CD8^+$ T cells at the indicated E: T ratios. After 24 h ~ 48 h, nonadherent tumor cells and T cells were washed away by PBS. Tumor cell viability was assessed using flow cytometry. Data were normalized to parallel cultures in the absence of T cells.

### Flow cytometry analysis

Single cell suspensions of tumor tissues were isolated as previously published[57]. Briefly, tumors were macerated into small pieces using a razor blade and incubated for 45 min at 37 °C in collagenase-containing buffer comprised of 100 U/ml collagenase type IV (Worthington, no. LS004186), 50 μg/ml of DNAase I (Worthington, no. LS006331) and 10% FBS in RPMI-1640 medium. After incubation, cells were treated with ACK RBC lysis buffer and passed through a 70 μM cell strainer to remove debris. All cells were resuspended in FACS buffer. Single cell suspensions were initially incubated with CD16/CD32 antibodies to block FcγRII/III receptors for 10 min at 4 °C and stained with antibodies for 30 min at 4 °C. Cells were then washed and resuspended in 7-AAD viability staining solution. For intracellular staining, cells were fixed and permeabilized using the Foxp3 Fix/Perm buffer set (eBioscience, no.00-5521-00) according to the manufacturer's protocol. The samples were acquired on a BD FACSCanto and analyzed using FlowJo V10. The antibodies are listed in Supplementary Table 1.

### Western Blotting

Western blotting was performed as previously described[58]. Briefly, cell lysates were prepared using lysis buffer containing HEPES (pH 7.0) (Life Technologies, no.15630080), 150 mM NaCl, 1% NP-40, 1 mM EDTA, 50 mM NaF, 10 mM b-glycerophosphate, 10 nM calyculin A, 1 mM $Na_3VO_4$, and protease inhibitors and normalized by protein concentrations using the Bradford method (Bio-Rad). Protein samples were separated on 10% SDS-PAGE and transferred to PVDF membrane (Millipore). Membranes were blocked in TBST containing 5% non-fat milk, incubated with primary antibodies according to the antibody manufacturer's instructions, followed by incubation with horseradish peroxidase-conjugated goat anti-rabbit or anti-mouse IgG and enhanced chemiluminescence detection.

### Lipid peroxidation measurement

Cells were seeded into 12-well plates incubated with 5 μM BODIPY 665/676 (Thermo Fisher, no. B3932) or BODIPY 581/591 C11 (Thermo Fisher, no. D3861) for 30 min at 37 °C after various treatments as indicated. Cells were harvested using trypsin-EDTA and washed twice in PBS. For measured lipid peroxidation in tumor cells with or without $CD8^+$ T cells, pretreated tumor cells were seeded into 12-well plates and cocultured activated $CD8^+$T cells for 24 h. Cells were collected by trypsinization after BODIPY incubation and labeled with FITC- or APC/Cy7-labeled anti-mouse or human CD45 antibodies, respectively, for 30 min. Lipid peroxidation was assessed using a BD FACS Canto flow cytometer. A minimum of 10000 single cells were analyzed per well.

### RNA-seq

RNA was isolated from cell pellets or tumors using the RNeasy mini kit from Qiagen (no.74104). RNA quality (RI*n* > 9) was confirmed using the TapeStation 4200 system (Agilent Technologies). Preparation of RNA library and transcriptome sequencing were conducted by Novogene Co., LTD (Sacramento, CA). 250 ~ 300 bp insert cDNA library was constructed according to the manufacturer's instructions (Illumina Platform, PE150 Q30 ≥ 80%). Pair-end sequencing with reads of 150 bp reads was performed on an Illumina HiSeq 2000. Sequencing reads were mapped to the UCSC mm10 reference genome using STAR version 2.7.0 f, and the differential expression analysis was performed with RSEM version 1.3.0. GSVA (R package) transforms the gene expression matrix of all samples into enrichment scores to quickly visualize how the gene sets enrichment change. Similarly, the 50 murine reference Hallmark gene sets were accessible through 'msigdbr' package. The kcdf parameter is Gaussian and method is GSVA. To show the varied Hallmark gene sets, the GSVA score of DMSO group was compared to which of the only BRQ treatment group using R package 'limma', by setting $P$ value < 0.05 and retaining gene sets with higher log2 fold change. Enrichment analyses were performed using 1,000 gene set permutations, a weighted enrichment statistic, the Signal2Noise ranking metric, and gene set minimum and maximum sizes of 15 and 500, respectively.

### Immunofluorescence

For Immunofluorescence staining, fresh cut paraffin sections were rehydrated using 2 series of xylene, 2 series of 100% ethanol and then 2 series of 95% ethanol. After washing with water for 5 minutes, antigen retrieval was performed using SignalStain® EDTA Unmasking Solution for DHODH staining following manufacture's instruction or using Antigen Retrieval CITRA Plus for 4-HNE as previously described[20]. Sections were blocked using 1% BSA in PBS for 30 minutes and then primary antibodies (DHODH Polyclonal antibody, Proteintech 14877-1-AP; Anti-4 Hydroxynonenal antibody, abcam ab46545; Cox2 antibody, Cell Signaling Technology #12282) were used at 1:100 dilution for DHODH,1:300 for 4-HNE and 1:200 for Cox2 antibodies. Primary antibody incubation was performed at 4 °C overnight. Alexa fluor secondary antibodies (Invitrogen) were used, then slides were mounted with Prolong Diamond Antifade Mountant with DAPI (Invitrogen). Images were taken using Olympus BX53F microscope, Olympus DP80 digital camera, and CellSens Standard software. Quantitative analysis for immunofluorescence staining was performed in 3 non-overlapping fields (200× magnification) for each sample using Fiji software to measure the percentage of positive area.

### Metabolomics

M14 and D4M cells were treated with DMSO or BRQ at indicated concentrations for 24 ~ 48 h. Cells were washed twice with ice cold PBS, and the final pellets were resuspended in 80% cold methanol and incubated at -80 °C for 15 min. The lysates were centrifuged at 16000 x g for 5 min at 4 °C and supernatants were collected and kept on dry ice. The pellet was re-extracted two times in 500 μL 80% methanol then centrifuged at 16000 x g for 5 min at 4 °C. The pooled supernatants were dried to completion by speedVac (ThermoFisher). Dried sample pellets were resuspended in HPLC-grade water (20 μL) and centrifuged at 20,000 × g for 5 minutes to remove insoluble material. Following centrifugation, 16 μL of supernatant was transferred to virgin polypropylene autosampler vials, capped, and placed on dry ice. Supernatants (5 μL) were injected and analyzed using a hybrid 6500 QTRAP triple quadrupole mass spectrometer (AB/SCIEX) coupled to a Prominence UFLC HPLC system (Shimadzu) via selected reaction monitoring (MRM). ESI voltage was +4,950 V in positive ion mode and

−4900 V in negative ion mode with polarity switching. A dwell time of 3 ms per SRM transition was used. Approximately 10 to 12 datapoints were acquired per detected metabolite. Q1/Q3 SRM transitions were developed to target both the unlabeled and labeled isotopomer forms of each tested metabolite in either positive or negative mode. Samples were delivered to the mass spectrometer via hydrophilic interaction chromatography (HILIC) using a 4.6 mm i.d. × 10 cm Amide XBridge column (Waters) at 400 µL/minute using a chilled autosampler. Gradients were run starting from 85% buffer B (HPLC-grade acetonitrile) to 42% B from 0 to 5 minutes; 42% B to 0% B from 5 to 16 minutes; 0% B was held from 16 to 24 minutes; 0% B to 85% B from 24 to 25 minutes; and 85% B was held for 7 minutes to reequilibrate the column. Buffer A was comprised of 20 mmol/L ammonium hydroxide/20 mmol/L ammonium acetate (pH = 9.0) in 95:5 water:acetonitrile. Peak areas from the total ion current for each metabolite SRM transition were integrated using MultiQuant v3.0 software (AB/SCIEX).

### Lipidomics

D4M cells were treated with DMSO, 1 µM BRQ, 300 µM CDP-Choline, or BRQ with CDP-Choline for 24 h. Following trypsinization, cells were collected by centrifugation and washed twice in PBS. 4 ×$10^6$ cells were resuspended in 200 µL PBS and then 1.5 mL methanol followed by addition of 5 mL Methyl tert-butyl ether (MTBE) buffer (Sigma, no.306975). The lysates were incubated for 1 h at room temperature with shaking. 1.25 mL of LC/MS grade water was added, and centrifuged at 1000 x *g* for 10 min. The MTBE upper phase was removed to a new tube and the aqueous phase was re-extracted with a 2 mL mixture of MTBE: methanol: water (10/3/2.5). Following centrifugation at 1000 x g, the upper phase was collected, and the combined MTBE phases were dried under vacuum at room temperature.

Samples were resuspended in 35 µL of 1:1 LC/MS-grade isopropanol:methanol and analyzed by liquid chromatography coupled to tandem mass spectrometry as described previously[59]. 1.5 µL samples were injected into a Cadenza 150 mm × 2 mm 3 µm C18 column (Imtakt) heated to 40 °C using a 1100 quaternary pump HPLC with room temperature autosampler (Agilent). Lipids were resolved using a linear gradient from 32% to 97% of buffer B for 22 min at 240 µL/min. Buffer A was 59.9% acetonitrile, 40% water plus 10 mM ammonium formate/0.1% formic acid, and buffer B was 90% isopropanol, 10% acetonitrile plus 10 mM ammonium formate/0.1% formic acid. Lipids were analyzed using a high-resolution hybrid QExactive HF Orbitrap mass spectrometer (Thermo) in data-dependent acquisition mode (Top 8) with positive/negative ion polarity switching. Data were acquired from m/z 225-1450 in MS1 mode with a resolution set to 70,000 for MS1 and 35,000 for MS2. MS1 and MS2 target values were set to 5e5 and 1e6, respectively. Lipid species were identified and quantified using LipidSearch 4.1.30 software (Thermo) using an internal database of ≥ 20 main lipid classes and ≥ 80 subclasses. To confirm the linearity of each lipid quantified, a pooled sample was generated by mixing 5 µL of each sample. This sample was diluted with 1:1 isopropanol:methanol to produce 0.3x- and 0.1x-pooled samples, and these dilutions and a blank were analyzed on the mass spectrometer. Data from mass spectrometry was normalized to a constant sum of 1000 using Metaboanalyst or manually normalized by sum using Microsoft Excel. Heat maps were generated using Metaboanalyst website, volcano plots and statistics were produced using Graphpad PRISM.

### Spatial transcriptomics (ST) data analysis

To investigate the relevance of spatial distribution between DHODH and $CD8^+$ T cells within the tumor microenvironment, spatial transcriptomics analysis was performed on public intestinal and ovarian cancer ST data processed by the 10X Genomics Visium platform. Feature/barcode matrix (filtered) and spatial imaging data were downloaded from the 10X website (https://www.10xgenomics.com/resources/datasets). The Space Ranger output files were processed with the SCTransform function using the 'Seurat' package in R software 4.3.0. The AddModuleScore method was used to calculate signature scores of cytotoxic T lymphocyte (CTL) (based on five genes, CD8A, CD8B, GZMA, GZMB, and PRF1), T cell receptor signaling, and interferon gamma signaling (based on the GSEA Database). These scores were scaled based on (each.score-min.score) / (max.score-min.score) and visualized by SpatialFeaturePlot. ST spots were separated into two groups of DHODH negative and DHODH high expression, of which the cutoff is set as 1.

We also analyzed Slide-seq v.2 spatial sequencing data of human melanoma metastasis specimens[31] (GSM6657936) and obtained melanoma single-cell transcriptome data[60] (GSE174401) for cell type annotation. Using the RCTD pipeline (v.1.2.0)[61] within the R package spacexr, we utilized the reference single-cell transcriptome dataset to learn expression profiles for each annotated cell type. These profiles were then applied to deconvolve cell-type proportions at each location in the spatial single-cell data. Based on these inferred cell types, we calculated the average distance of the 10 T cells closest to the tumor cell. The relationship between DHODH expression in the tumor cell and the average of its distance to T cells was analyzed using Student's *t*-test, based on the median DHODH expression.

### Quantification and statistical analysis

Data are generally plotted as mean ± SEM. No statistical methods were used to pre-determine sample sizes. GraphPad Prism V9 was used for data analysis and graphic representations. Comparisons between two groups were performed with two-tailed Student's t-test. Comparisons among more than two groups were performed with ANOVA analysis followed by Tukey's test. *P* values less than 0.05 were considered significant.

### Reporting summary

Further information on research design is available in the Nature Portfolio Reporting Summary linked to this article.

## Data availability

The transcriptomics data generated in this study have been deposited in the Gene Expression Omnibus database under the accession code GSE: 243486. The mass spectrometry data generated in this study have been deposited in the MetaboLights repository under accession code MTBLS12334. Public intestinal and ovarian cancer spatial transcriptomics feature / barcode matrix (filtered) and spatial imaging data were downloaded from the 10X Genomics Visium website (https://www.10xgenomics.com/datasets). Spatial sequencing data of human melanoma metastasis specimens (GSM6657936) and melanoma single-cell transcriptome data (GSE174401) were downloaded from the public database (https://www.ncbi.nlm.nih.gov/geo/query/acc.cgi?acc=GSE174401) and (https://www.ncbi.nlm.nih.gov/geo/query/acc.cgi?acc=GSM6657936). Source data are provided with this paper.

## References

1. Hanahan, D. & Weinberg, R. A. Hallmarks of cancer: the next generation. *Cell* **144**, 646–674 (2011).
2. van Weverwijk, A. & de Visser, K. E. Mechanisms driving the immunoregulatory function of cancer cells. *Nat. Rev. Cancer* **23**, 193–215 (2023).
3. Spranger, S. & Gajewski, T. F. Mechanisms of tumor cell–intrinsic immune evasion. *Annu. Rev. Cancer Biol.* **2**, 213–228 (2018).
4. Martinez-Reyes, I. et al. Mitochondrial ubiquinol oxidation is necessary for tumour growth. *Nature* **585**, 288–292 (2020).
5. Bajzikova, M. et al. Reactivation of dihydroorotate dehydrogenase-driven pyrimidine biosynthesis restores tumor growth of respiration-deficient cancer cells. *Cell Metab.* **29**, 399–416.e310 (2019).

6. White, R. M. et al. DHODH modulates transcriptional elongation in the neural crest and melanoma. *Nature* **471**, 518–522 (2011).
7. Sykes, D. B. et al. Inhibition of dihydroorotate dehydrogenase overcomes differentiation blockade in acute myeloid leukemia. *Cell* **167**, 171–186.e115 (2016).
8. Mathur, D. et al. PTEN regulates glutamine flux to pyrimidine synthesis and sensitivity to dihydroorotate dehydrogenase inhibition. *Cancer Discov.* **7**, 380–390 (2017).
9. Brown, K. K., Spinelli, J. B., Asara, J. M. & Toker, A. Adaptive reprogramming of de novo pyrimidine synthesis is a metabolic vulnerability in triple-negative breast cancer. *Cancer Discov.* **7**, 391–399 (2017).
10. Koundinya, M. et al. Dependence on the pyrimidine biosynthetic Enzyme DHODH is a synthetic lethal vulnerability in mutant KRAS-driven cancers. *Cell Chem. Biol.* **25**, 705–717.e711 (2018).
11. Wang, X. et al. Targeting pyrimidine synthesis accentuates molecular therapy response in glioblastoma stem cells. *Sci. Transl Med.* **11**, eaau4972 (2019).
12. Li, L. et al. Identification of DHODH as a therapeutic target in small cell lung cancer. *Sci. Transl Med.* **11**, 10.1126/scitranslmed.aaw7852 (2019).
13. Gwynne, W. D. et al. Cancer-selective metabolic vulnerabilities in MYC-amplified medulloblastoma. *Cancer Cell* **40**, 1488–1502 e1487 (2022).
14. Shi, D. D. et al. De novo pyrimidine synthesis is a targetable vulnerability in IDH mutant glioma. *Cancer Cell* **40**, 939–956.e916 (2022).
15. Jenkins, M. H. et al. Multiple murine BRaf(V600E) melanoma cell lines with sensitivity to PLX4032. *Pigment Cell Melanoma Res.* **27**, 495–501 (2014).
16. Kondo, T. Selective eradication of pluripotent stem cells by inhibiting DHODH activity. *Stem Cells* **39**, 33–42 (2021).
17. Bork, E., Vest, S. & Hansen, H. H. A phase I clinical and pharmacokinetic study of brequinar sodium, DUP 785 (NSC 368390), using a weekly and a biweekly schedule. *Eur. J. Cancer Clin. Oncol.* **25**, 1403–1411 (1989).
18. Schwartsmann, G. et al. Phase I study of brequinar sodium (NSC 368390) in patients with solid malignancies. *Cancer Chemother. Pharm.* **25**, 345–351 (1990).
19. Stockwell, B. R. Ferroptosis turns 10: Emerging mechanisms, physiological functions, and therapeutic applications. *Cell* **185**, 2401–2421 (2022).
20. Mao, C. et al. DHODH-mediated ferroptosis defence is a targetable vulnerability in cancer. *Nature* (2021).
21. Christian, S. et al. The novel dihydroorotate dehydrogenase (DHODH) inhibitor BAY 2402234 triggers differentiation and is effective in the treatment of myeloid malignancies. *Leukemia* **33**, 2403–2415 (2019).
22. Cao, L. et al. Targeting of hematologic malignancies with PTC299, A novel potent inhibitor of dihydroorotate dehydrogenase with favorable pharmaceutical properties. *Mol. Cancer Ther.* **18**, 3–16 (2019).
23. Zhou, J. et al. ASLAN003, a potent dihydroorotate dehydrogenase inhibitor for differentiation of acute myeloid leukemia. *Haematologica* **105**, 2286–2297 (2020).
24. Wang, W. et al. CD8+T cells regulate tumour ferroptosis during cancer immunotherapy. *Nature* **569**, 270–274 (2019).
25. Lee, J. Y. et al. Polyunsaturated fatty acid biosynthesis pathway determines ferroptosis sensitivity in gastric cancer. *Proc. Natl Acad. Sci. USA* **117**, 32433–32442 (2020).
26. Conrad, M. & Pratt, D. A. The chemical basis of ferroptosis. *Nat. Chem. Biol.* **15**, 1137–1147 (2019).
27. Qiu, B. et al. Phospholipids with two polyunsaturated fatty acyl tails promote ferroptosis. *Cell* **187**, 1177–1190.e1118 (2024).
28. DeLong, C. J., Shen, Y. J., Thomas, M. J. & Cui, Z. Molecular distinction of phosphatidylcholine synthesis between the CDP-choline pathway and phosphatidylethanolamine methylation pathway. *J. Biol. Chem.* **274**, 29683–29688 (1999).
29. Liao, P. et al. CD8(+) T cells and fatty acids orchestrate tumor ferroptosis and immunity via ACSL4. *Cancer Cell* **40**, 365–378.e366 (2022).
30. Lo, J. A. et al. Epitope spreading toward wild-type melanocyte-lineage antigens rescues suboptimal immune checkpoint blockade responses. *Sci Transl Med.* **13** (2021).
31. Wang, Y. et al. Multimodal single-cell and whole-genome sequencing of small, frozen clinical specimens. *Nat. Genet* **55**, 19–25 (2023).
32. Wu, X. et al. Comprehensive characterization of tumor microenvironment in colorectal cancer via molecular analysis. *Elife* **12**, e86032 (2023).
33. Catanzaro, E., Demuynck, R., Naessens, F., Galluzzi, L. & Krysko, D. V. Immunogenicity of ferroptosis in cancer: a matter of context? *Trends Cancer* **10**, 407–416 (2024).
34. Tang, D., Kepp, O. & Kroemer, G. Ferroptosis becomes immunogenic: implications for anticancer treatments. *Oncoimmunology* **10**, 1862949 (2020).
35. Wiernicki, B. et al. Cancer cells dying from ferroptosis impede dendritic cell-mediated anti-tumor immunity. *Nat. Commun.* **13**, 3676 (2022).
36. Song, J. et al. The deubiquitinase OTUD1 enhances iron transport and potentiates host antitumor immunity. *EMBO Rep.* **22**, e51162 (2021).
37. Mullen, N. J. et al. DHODH inhibition enhances the efficacy of immune checkpoint blockade by increasing cancer cell antigen presentation. *eLife* **12**, RP87292 (2024).
38. Mishima, E. et al. DHODH inhibitors sensitize to ferroptosis by FSP1 inhibition. *Nature* **619**, E9–E18 (2023).
39. Mao, C., Liu, X., Yan, Y., Olszewski, K. & Gan, B. Reply to: DHODH inhibitors sensitize to ferroptosis by FSP1 inhibition. *Nature* **619**, E19–E23 (2023).
40. von Krusenstiern, A. N. et al. Identification of essential sites of lipid peroxidation in ferroptosis. *Nat. Chem. Biol.* **19**, 719–730 (2023).
41. Wright, M. M. & McMaster, C. R. PC and PE synthesis: mixed micellar analysis of the cholinephosphotransferase and ethanolaminephosphotransferase activities of human choline/ethanolamine phosphotransferase 1 (CEPT1). *Lipids* **37**, 663–672 (2002).
42. Tian, S. et al. Human CTP:phosphoethanolamine cytidylyltransferase: enzymatic properties and unequal catalytic roles of CTP-binding motifs in two cytidylyltransferase domains. *Biochem Biophys. Res Commun.* **449**, 26–31 (2014).
43. Tie, A. & Bakovic, M. Alternative splicing of CTP:phosphoethanolamine cytidylyltransferase produces two isoforms that differ in catalytic properties. *J. Lipid Res* **48**, 2172–2181 (2007).
44. Spina, R. et al. DHODH inhibition impedes glioma stem cell proliferation, induces DNA damage, and prolongs survival in orthotopic glioblastoma xenografts. *Oncogene* **41**, 5361–5372 (2022).
45. Rossmann, M. P. et al. Cell-specific transcriptional control of mitochondrial metabolism by TIF1gamma drives erythropoiesis. *Science* **372**, 716–721 (2021).
46. Boukalova, S. et al. Dihydroorotate dehydrogenase in oxidative phosphorylation and cancer. *Biochim Biophys. Acta Mol. Basis Dis.* **1866**, 165759 (2020).
47. Zhou, Y. et al. DHODH and cancer: promising prospects to be explored. *Cancer Metab.* **9**, 22 (2021).
48. Moore, M. et al. Multicenter phase II study of brequinar sodium in patients with advanced gastrointestinal cancer. *Invest N. Drugs* **11**, 61–65 (1993).

49. Maroun, J. et al. Multicenter phase II study of brequinar sodium in patients with advanced lung cancer. *Cancer Chemother. Pharm.* **32**, 64–66 (1993).
50. Li, C. et al. A novel series of teriflunomide derivatives as orally active inhibitors of human dihydroorotate dehydrogenase for the treatment of colorectal carcinoma. *Eur. J. Med. Chem.* **238**, 114489 (2022).
51. McDonald, G. et al. Selective vulnerability to pyrimidine starvation in hematologic malignancies revealed by AG-636, a novel clinical-stage inhibitor of dihydroorotate dehydrogenase. *Mol. Cancer Ther.* **19**, 2502–2515 (2020).
52. Sanders, S. & Harisdangkul, V. Leflunomide for the treatment of rheumatoid arthritis and autoimmunity. *Am. J. Med. Sci.* **323**, 190–193 (2002).
53. Scherer, S. et al. Pyrimidine de novo synthesis inhibition selectively blocks effector but not memory T cell development. *Nat. Immunol.* **24**, 501–515 (2023).
54. Colligan, S. H. et al. Inhibiting the biogenesis of myeloid-derived suppressor cells enhances immunotherapy efficacy against mammary tumor progression. *J. Clin. Invest.* **132**, e158661 (2022).
55. Xu, X., Williams, J. W., Gong, H., Finnegan, A. & Chong, A. S. Two activities of the immunosuppressive metabolite of leflunomide, A77 1726. Inhibition of pyrimidine nucleotide synthesis and protein tyrosine phosphorylation. *Biochem Pharm.* **52**, 527–534 (1996).
56. Xu, X. et al. In vitro and in vivo mechanisms of action of the antiproliferative and immunosuppressive agent, brequinar sodium. *J. Immunol.* **160**, 846–853 (1998).
57. Kim, S. H. et al. Phenformin inhibits myeloid-derived suppressor cells and enhances the anti-tumor activity of PD-1 blockade in melanoma. *J. Invest Dermatol* **137**, 1740–1748 (2017).
58. Yuan, P. et al. Phenformin enhances the therapeutic benefit of BRAF(V600E) inhibition in melanoma. *Proc. Natl Acad. Sci. USA* **110**, 18226–18231 (2013).
59. Breitkopf, S. B. et al. A relative quantitative positive/negative ion switching method for untargeted lipidomics via high resolution LC-MS/MS from any biological source. *Metabolomics* **13**, 10.1007/s11306-016-1157-8 (2017).
60. Smalley, I. et al. Single-cell characterization of the immune microenvironment of melanoma brain and leptomeningeal metastases. *Clin. Cancer Res.* **27**, 4109–4125 (2021).
61. Cable, D. M. et al. Cell type-specific inference of differential expression in spatial transcriptomics. *Nat. Methods* **19**, 1076–1087 (2022).
62. Teng, D. https://BioRender.com/n23p463 (2025).


## Acknowledgements

We thank and members of the Zheng Lab for helpful discussion on the manuscript. This work is supported by US National Institutes of Health (NIH) R21CA227588, R01CA219814, R01CA266875, R01CA276448, Department of Defense (DOD) ME220187, and the Melanoma Research Alliance (to B.Z.), NIH R50CA232985 (to Y.Z.); and NIH R01CA290780 (to Y.Z. and B.Z.). B.Z. is the Debra Black Chair of Melanoma Research at Cedars-Sinai Medical Center.

## Author contributions

D.T., K.D.S., and B.Z. designed experiments; D.T., K.D.S., H.W., F.R.A. and Y.Z. performed experiments; D.T., K.D.S., R.W., A.Z., Z.N. and L.C. performed computational analysis; L.G., J.M.A., Y.Z. and B.Z. provided supervision; all of the authors interpreted data and discussed results; and D.T., K.D.S., and B.Z. wrote the paper with input from all of the authors.

## Competing interests

The authors declare no competing interests.

## Additional information

**Supplementary information** The online version contains supplementary material available at https://doi.org/10.1038/s41467-025-59307-y.

**Correspondence** and requests for materials should be addressed to Bin Zheng.

**Peer review information** *Nature Communications* thanks Eun-Woo Lee, Chao Mao and the other, anonymous, reviewer(s) for their contribution to the peer review of this work. A peer review file is available.